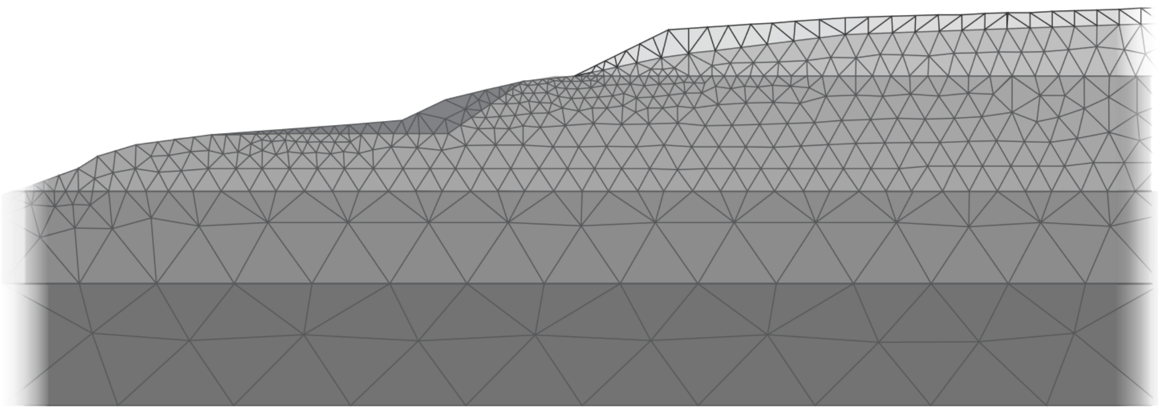

The Effects of Severe Rainfall on the Stability of Natural Slopes

A numerical analysis of a slope in Hjärtum – Lilla Edet

Master’s Thesis in the Master’s Programme Infrastructure and Environmental Engineering

TOBIAS BRANDELL
ALBIN SELLDÉN

DEPARTMENT OF ARCHITECTURE AND CIVIL ENGINEERING
CHALMERS UNIVERSITY OF TECHNOLOGY
Gothenburg, Sweden 2022
www.chalmers.se

MASTER'S THESIS ACEX30

The Effects of Severe Rainfalls on the Stability of Natural Slopes

A numerical analysis of a slope in Hjärtum – Lilla Edet

Master's Thesis in the Master's Programme Infrastructure and Environmental Engineering

TOBIAS BRANDELL
ALBIN SELLDÉN

CHALMERS

Department of Architecture and Civil Engineering
Division of Geology and Geotechnics
CHALMERS UNIVERSITY OF TECHNOLOGY
Göteborg, Sweden 2022

The Effects of Severe Rainfalls on the Stability of Natural Slopes

A numerical analysis of a slope in Hjärtum – Lilla Edet

Master's Thesis in the Master's Programme Infrastructure and Environmental Engineering

TOBIAS BRANDELL
ALBIN SELLDÉN

Examensarbete ACEX30
Institutionen för arkitektur och samhällsbyggnadsteknik
Chalmers tekniska högskola, 2022

Department of Architecture and Civil Engineering
Division of Geology and Geotechnics
Chalmers University of Technology
SE-412 96 Göteborg
Sweden
Telephone: + 46 (0)31-772 1000

Cover:
A representation of the geometry and mesh of the analysed slope in Hjärtum, Lilla Edet.

Department of Architecture and Civil Engineering
Göteborg, Sweden, 2022

The Effects of Severe Rainfalls on the Stability of Natural Slopes
A numerical analysis of a slope in Hjärtum – Lilla Edet

Master’s thesis in the Master’s Programme Infrastructure and Environmental Engineering

TOBIAS BRANDELL
ALBIN SELLDÉN

Department of Architecture and Civil Engineering
Division of Geology and Geotechnics
Chalmers University of Technology

ABSTRACT
The effect of global warming tends to cause more frequent extreme weather events across the planet. These types of extreme weathers may present themselves as more intense and long-lasting rainfalls which have proved to be critical in terms of slope stability. As a rainfall occurs, the negative pore pressure of an unsaturated of partially saturated slope reduces hence the slope loses part of its stability capacity. The negative pore pressure, known as suction, is directly correlating to the safety factor of a slope. Ultimately, this means that when the suction reduces, the safety reduces and vice versa. The aim of the study is to examine how future rainfalls will affect the stability of a natural slope during an entire month. The goal is for the report to act as a framework for future studies regarding slope stability as a component of evolving precipitation conditions. To exemplify this framework, an existing slope in Hjärtum, Lilla Edet, adjacent to Göta älv has been investigated. Prior to this study, an analysis has been conducted by SWECO to evaluate the stability at different sections of the slope.

To evaluate how future precipitation will evolve, existing studies for Västra Götaland have been utilized and adapted to the specific case Hjärtum, Lilla Edet. To determine whether the month with the single most extreme rainfall or the month with the most total precipitation was more critical for the slope stability, two months in the reference period 1961-2010, matching those descriptions, were identified. The rainfalls from the reference period were adjusted to correspond with each scenario. The slope was modelled in the software PLAXIS 2D and the precipitation was defined as an external infiltration subtracted with the evapotranspiration. In total, four calculations for each scenario were performed, namely the reference case, followed by the time-period intervals: 2011-2040, 2041-2070, and lastly 2071-2100.

It was found that the precipitation will increase significantly until the year 2100 with short duration extreme rainfalls and precipitations during the winter being the most affected. Furthermore, the safety factor of slopes similar to the one in Hjärtum, are in great risk of being significantly impacted by the increasing severity of the situation. Lastly it was concluded that the most critical future scenario is one where more prolonged periods of rain unfold.

Key words: **Slope stability, suction, precipitation, Göta älv, climate change**

Contents

Preface

The following report is authored by two students from the master's programme Infrastructure and Environmental Engineering at Chalmers University of Technology during the spring semester 2022. The study was conducted within the division of Geology and Geotechnics with supervision of Ayman Abed, Senior Lecturer at the department of Geotechnics. The project has been carried out in collaboration with SWECO AB.

First, we would like to thank our supervisor and own numerical guru Ayman Abed, who has been providing valuable support and guidance throughout the project. Further, we would like to acknowledge our examiner Minna Karstunen for raising interest and curiosity about geotechnics and the subject of slope modelling. Additionally, we want to express our gratitude to Per Lager and Hanna Blomén at SWECO for their involvement and support for our study. Finally, we would like to thank Per Nylander at the Swedish Geological Institute for providing useful information and data for the project.

Chalmers University of Technology
Göteborg June 2022

Tobias Brandell
Albin Selldén

Notations

Roman upper-case letters

E'	Stiffness modulus
K_0	Ratio between horizontal and vertical stress
L_v	Latent heat of vaporization
R_{ij}	Intensity in litres per hectar
R_v	Universal gas constant
S	Matric suction
S_e	Effective saturation
S_t	Total suction
T_k	Temperature in degrees Kelvin

Roman lower-case letters

c	Soil cohesion
e_s	Saturation water vapour pressure
h	Matric potential
k_w	Coefficient of permeability
m	Asymmetry value
m_b	Bishop effective stress parameter
n	Pore size distribution
p_a	Pore air pressure
p_w	Pore water pressure
s	Standard deviation
s_u	Field vane strength
t_j	Duration in minutes

Greek letters

α	Air-entry value
θ	Water content
θ_r	Residual water content
θ_s	Saturated water content
π	Osmotic suction
σ	Total stress
σ'	Effective stress
τ_i	Time in months
υ	Poisson's ratio
φ	Friction angle
χ	Matric suction coefficient

Abbreviations

CH_4	Methane
CO_2	Carbon dioxide
CPT	Cone penetration test
CRS	Constant rate of strain
FEM	Finite element method
GHG	Greenhouse gas

Msf	Safety factor at convergence
N_2O	Nitrous oxide
SF	Safety factor
SO_2	Sulfur dioxide
SWCC	Soil water characteristic curve

List of figures

List of tables

1 Introduction

This chapter acts as an introduction to the subject of slope stability and the consequences that climate change imposes. Furthermore, the scope, limitations, and considerations of the study will be presented.

1.1 Background

Climate change has become more and more noticeable in the past few decades with implications such as temperature increase, unstable weather conditions and long periods of drought [1]. In the summer of 2021, several extreme rainfall events occurred around western and northern Europe with fatal consequences [2], [3]. The disastrous aftermath emerged due to soil failure and infrastructural collapses which lead to evacuation of entire communities. The trend of more frequent extreme weather events indicates that challenges regarding soil stability and infrastructure resilience are only going to be even more complicated in the near future. During the last 100 years, more than 55 landslides have occurred in Sweden according to the Swedish Commission on Climate and Vulnerability [4]. Some of the more vulnerable locations have proved to be slopes and geological formations along Göta älv. The soil along the river mainly consists of marine clays which are particularly susceptible to sliding.

It is generally predicted that the safety factor of slopes will decrease with increasing amounts of precipitation. There have been international studies to evaluate such cases of which one is a study performed by Viet, T [5]. In this study the effects of heavy rainfalls on cut slopes in the northern part of Vietnam were examined. The study proved the magnitude of the effect that rain can have on the stability of a slope. There is a scarcity of similar studies made for Sweden and its neighbouring countries and how the location-specific soils are affected during rainfalls. It is known that the phenomenon suction is a crucial parameter while analysing hydrological conditions in soils such as clay. Suction ultimately increases the resisting forces, and thus also the safety factor of a slope, and is only present in the partially or unsaturated zone of a soil. The more saturated the zone becomes, the less suction it will experience. Thus, when rainfalls occur and saturates the zone, the suction and by extension, safety factor, decreases. To calculate the stability of a slope with the influence of suction can be much more complex than to simply ignore the suction, i.e., assuming full saturation. This is seen as the conservative alternative since it is effectively evaluating the worst-case scenario. However, it can in some cases lead to confusing results where a safety factor below 1 is obtained while the examined slope still stands. This indicates that the effect of the suction plays a critical role in the stability of the slope since without it, the slope would succumb to sliding. To not consider suction could be seen as conservative while designing a slope yet reckless to ignore while evaluating an existing natural slope. Being aware of which events can cause the suction to decrease to the point of failure can prove essential in slope stability and needs further investigation.

1.2 Problem description

As the climate evolves and becomes more difficult to predict, things which have been taken for granted may have to be re-evaluated. Climate change will not only bring more unpredictable temperature variations but also more intense and unpredictable rainfalls together with longer periods of drought. The effects of rainfalls can be catastrophic in many ways and natural geological formations such as slopes have proved heavily affected by this. When the possible effects have previously been examined, mostly fully saturated conditions have been applied [6], [7]. The reason for this is an uncertainty surrounding the long-term reliability of negative pore water pressure [8]. To instead use fully saturated conditions have been deemed more conservative although it does not always reflect reality. In Sweden, rainfalls last for a relatively short duration and are not overly intense at the present time. The stability of natural slopes could therefore be endangered with the increased severity of the situation as climate conditions change. Slopes that are in critical locations may have to be re-evaluated for future climate prognoses.

1.3 Aim and research questions

The aim is to examine how future rainfalls will affect the stability and safety factor of a natural slope during an entire month. The goal is that the report can be used as a framework for similar studies in the future. A slope in Hjärtum, located in the municipality Lilla Edet, will be investigated to exemplify the methodology and to evaluate the effect of future precipitation conditions on the stability of a natural slope. Prior to the study, SWECO had performed a stability analysis of the slope in Hjärtum and crucial parameters and geometries will be retrieved in cooperation with the company. The study will revolve around, yet is not limited to the following research questions:

- How will precipitation conditions in Västra Götaland evolve until the year 2100?
- To what extent will the safety factor of natural slopes be affected by the most extreme rainfall scenarios in the future compared to the most extreme rainfall scenarios today?
- Is the month with the single most extreme rainfall event or the month with the most total precipitation more critical for the stability of a slope?

1.4 Boundaries

The study will be limited to the effect that the single most extreme rainfall and the month with the most total precipitation have on the safety factor of a slope. Aspects that will be neglected include sea level rise and phenomena such as storms or earthquakes. Furthermore, the effects that snow and ice will have on the stability will not be considered. The simulation will solely be performed in the software PLAXIS 2D and calculated at three one-month periods which are 30 years apart, namely, 2040, 2070, and 2100. The weather predictions and slope stability simulations will revolve around areas in proximity to Göta älv in Västra Götaland. More specifically, Gothenburg will be used for weather data collection and the location Hjärtum, Lilla Edet, is where the studied slope is located. Furthermore, due to estimations and certain adjustments, the results will not necessarily, fully reflect reality of the specific location but rather exemplify possible future scenarios.

1.5 Ethical considerations

Ethical aspects have been considered to ensure that all communications throughout the study are approved for publishment. That means that all participants know for what purpose their information is intended for before they agree to share their knowledge. Also, anonymity is ensured to the point that no identifiable data is collected. Names that are published in the report are verified by each individual for usage. The author's responsibility is to ensure that the work is free of plagiarism as well as presenting the provided information correctly.

2
Theory

The following chapter will provide a theoretical background to certain key concepts and parameters regarding climate change and soil stability for the study. The concepts will include but are not limited to temperature increase, precipitation prognoses, safety factor of slopes, suction, and soil water characteristics curve.

2.1 Climate change

The United Nations defines climate change as "the long-term shift in temperature and weather patterns" [9]. Historically, the climate has been observed as a cyclic pattern with reoccurring periods of extreme heat and cold. The significant fluctuations in temperature can be explained by a multitude of both natural and humanitarian variations that have been influencing the climate. An essential contributor to natural climate change is the sun. The sun is the planet's source of energy and a fundamental parameter to the climate and its evolution. The intensity of the sun is constantly varying, however, since 1970 the net energy shows no increase in output [10]. Meanwhile, it has been concluded that it is from this time where the global surface temperature indicates the most rapid increase. Although the variation of solar activity contributes to climate change it is assumed to constitute a rather small role in the total contribution the last couple of decades [11]. Further natural causes to climate change include volcanic activity, changes of the earth's reflectivity, variations of the earth's orbit and rotation, changing of naturally occurring greenhouse gases, and more [12]. While natural causes cannot explain the climate change independently, the effect that human activity have had on the long-term global warming trend is undeniable at this point.

For almost two centuries it has been brought to scientists' attention that excessive emissions of greenhouse gases lead to atmospheric capturing of heat thus warming the planet [13]. The main greenhouse gases originating from human activity is carbon dioxide, methane gas, fluorinated gases, and nitrous dioxide [14]. These vary in terms of atmospheric content and heat capturing potential. While carbon dioxide accounts for 76% of the total GHG emitted, methane and nitrous dioxide adds up to 16% and 6% respectively. Methane gas holds a global warming impact 25 times more potent than carbon dioxide, although persisting in the atmosphere for a substantially shorter time. Nitrous dioxide is even more potent than methane with a global warming potential 300 times more than carbon dioxide. Similar to methane, nitrous oxide persists significantly shorter in the atmosphere than carbon dioxide. Lastly, fluorinated gases are a completely man-made greenhouse gas with a global warming potential ranging from 100 to 23 000 more than carbon dioxide [15]. However, only accounting for 2% of the total GHG emitted. Fluorinated gases include several substances with varying global warming potential, concentration, and lifetime [16].

2.1.1 Future predictions

In 2015, 196 international parties gathered in Paris to establish what would become the first ever universal legally binding global climate change agreement [17]. The objective of the agreement was to limit global warming by 2°C with the preferable limit of 1.5°C above the pre-industrial reference period 1850-1900. Despite the pursuit towards a globally sustainable climate program, the trend of a warmer planet seems to become an inevitable reality in the future. In 2021, the intergovernmental panel on climate change presented five different emission scenarios to project how the global surface temperature will evolve for short (2021-2040)-, medium (2041-2060)- and long-term (2081-2100) time frames [18].

The five different emission scenarios; SSP1-1.9, SSP1-2.6, SSP2-4.5, SSP3-7.0 and SSP5-8.5 are estimated for future projections until the year 2100, see Figure 2.1. The estimations are focused to the four different emissions: carbon dioxide, methane, nitrous dioxide, and sulfur dioxide. While scenarios SSP5-8.5 and SSP3-7.0 simulates high emission scenarios with considerable increase of CO_2, SSP2-4.5, SSP1-2.6 and SSP1-1.9 projects a reduction of CO_2 by the year of 2100, see Figure 2.1. For methane and nitrous dioxide, the high emission scenarios SSP3-7.0 and SSP5-8.5 estimates an increase by 2100 relative to current quantities while the remaining scenarios suggest a reduction. Lastly, the sulfur dioxide levels are projected to decline for all emission scenarios. A downward trend of sulfur dioxide levels has been observed for just over 30 years due to a combination of measures, one of them being a conversion of fuel in energy sectors. The traditional combustion fuel coal has been replaced with low-sulfur fuels such as natural gas hence reducing the levels of sulfur dioxide [19]. With even stricter regulations and the out-phasing of fossil fuels, the levels of sulfur dioxide are projected to reduce even further for future scenarios.

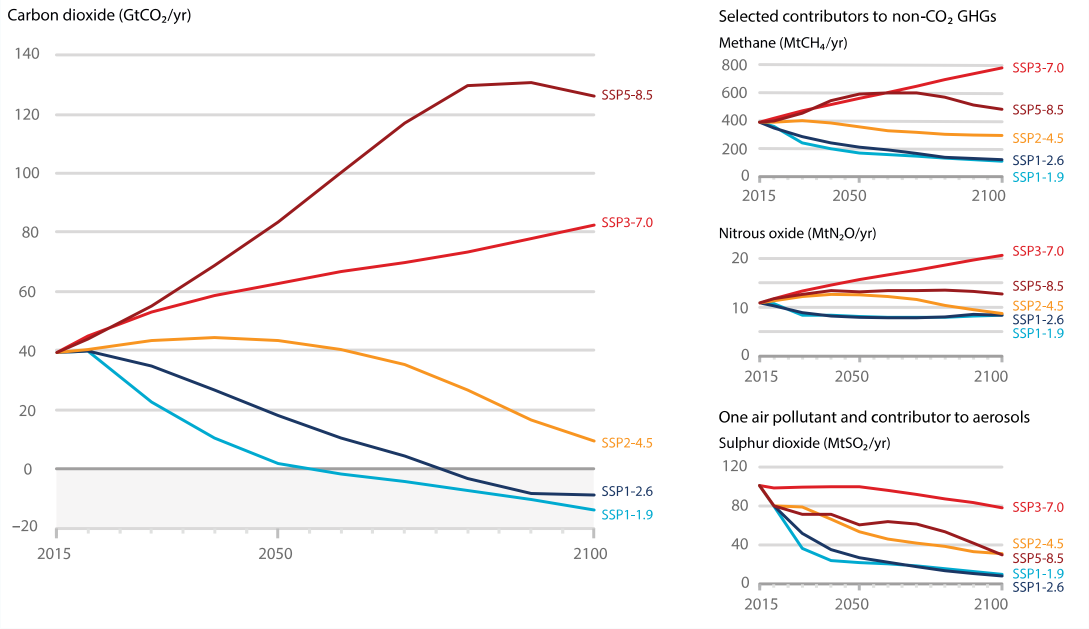

Figure 2.1. Emission scenarios for CO_2, CH_4, N_2O, and SO_2 until 2100 [18].

Figure 2.2 demonstrates a projected increase of the global surface temperature relative to the industrial baseline 1850-1900. The five different emission scenarios are displayed with the best estimated temperature represented as lines. The best-case scenario showed that by the long-term projection, 2081-2100, the temperature would *very likely* range between 1°C to 1.8°C from industrial baseline. This is provided that GHG emissions are drastically reduced, and carbon dioxide is declining to net zero towards 2050 with following years of negative net carbon dioxide emissions. Additionally, levels of methane and nitrous dioxide must significantly reduce in order to achieve the desirable temperature limit. The worst-case scenario indicates a temperature increase between 3.3°C to 5.7°C for the long-term projection with the best estimated temperature of 4.7°C by 2100, see Figure 2.2.

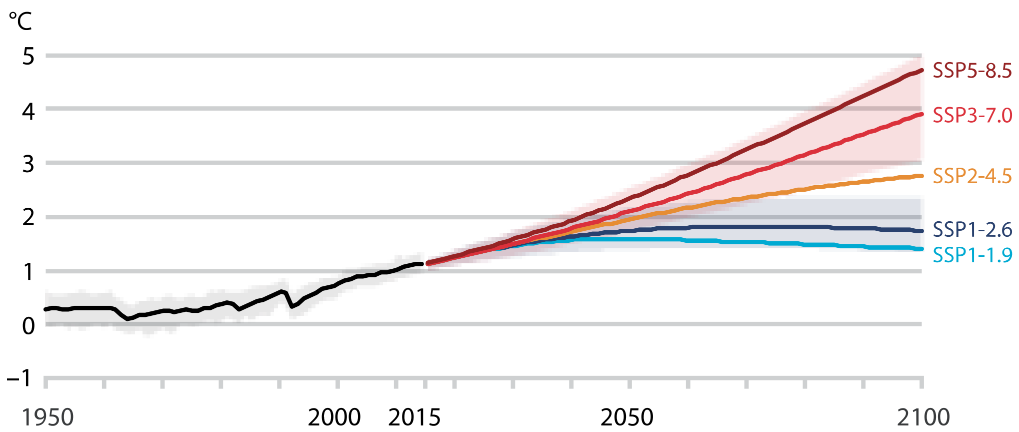

Figure 2.2. Projected temperature increase [18].

2.1.2 Consequences

In 2021, the average global surface temperature had risen 1.09°C from the pre-industrial baseline between 1850-1900. Besides this, it has been concluded that the last decade has been the warmest on record since temperature measurements began in 1880 [20]. An increased planetary temperature does not only entail melting ices and rising sea levels but also risks global weather patterns to be revised [21]. The trend of a warmer planet tends to cause more frequent extreme weather events such as heat waves, storms, drought, and floods. Climate change affects all regions in the world entailing different consequences for different geographical locations. In Europe, there are already significant climate variations within the continent and climate change will appear differently for particular regions. While southern and central Europe will experience more frequent heat waves, drought and forest fires, northern Europe will encounter significantly wetter conditions with more intense rainfalls [22]. This was noticeable in several parts of the continent in 2021, including in Sweden. The most severe case was a rainfall event in Gävle where 161mm of precipitation was measured during a single day in late August [23]. The flooding events in western Europe are another example of the type of devastating consequences this type of extreme weather may implicate. A study particularly focusing on the causes of the flooding events in western Europe claims that climate change directly correlates to the extreme weather that affected the region [24]. Moreover, the study suggests that a climate 1.2°C cooler than current temperature would reduce the risk of experiencing such an event by a factor between 1.2 and 9.

2.1.3 Precipitation conditions and prognosis

Historically, it has been shown that minimal fluctuations of the average global temperature affect the climate to a great extent. According to SMHI [25], an increase of 1°C would entail roughly a 7% intensification of daily extreme precipitation events. This correlates to Clausius Clapeyron's theory suggesting the relation between the amount of water vapor that air can hold at certain temperatures [26]. The relationship can be expressed as Equation 2.1 to describe the amount of water the atmosphere is capable of accommodating. T_k is the temperature in degrees Kelvin, e_s is the saturation water vapour pressure, L_v the latent heat of vaporization and R_v the universal gas constant [26].

$$\frac{\delta e_s}{\delta T_k} = \frac{L_v e_s}{R_v T_k^2} \tag{2.1}$$

The interval of duration and intensity of a rainfall can vary between barely noticeable to catastrophic. The different kinds of rainfalls are categorized by the reoccurrence time, i.e., the statistical likeliness to occur [27]. Furthermore, the duration does not necessarily have to be great for an unlikely rainfall, but the intensity would be more significant. Similarly, an unlikely rainfall scenario is not necessarily intense but can unfold during a longer duration. Often when discussed, certain rainfall scenarios are referred to as how often they are statistically plausible to occur. A 1-year rain is therefore a rain which is likely to occur roughly once a year. The intensity and duration of the rain are correlated according to Dahlström's formula where reoccurrence time and duration are used to determine the relative intensity, see Equation 2.2 [28]. The reoccurrence time, τ_i, is in months while the duration, Δt_j, is in minutes. The constant *190* is related to the statistics and weather conditions of a certain location and is, in this case, specific for Sweden. The factor *2* stabilizes the formula for longer duration rainfalls. Finally, the intensity, R_{ij}, is output as litres per second and hectar (l/s ha).

$$R_{ij} \approx 190 \sqrt[3]{\tau_i} \ln \frac{\Delta t_j}{\Delta t_j^{\,0.98}} + 2 \qquad 2.2$$

2.1.3.1 Evapotranspiration

Evapotranspiration is a physical process that describes the amount of water vapor that ascends into the atmosphere. Essentially, the process covers three mechanisms, the first being evaporation, i.e., water that directly evaporates from soil, water, snow, and ice. Secondly it includes transpiration, i.e., evaporation from microscopic pores in plants, and lastly interception, which is water that ultimately is evaporated after being intersected by vegetation and thus never reaching the ground [29]. The evapotranspiration rate varies with a multitude of parameters, including temperature, humidity, surface albedo, and wind thus differing significantly throughout the year. The highest evapotranspiration rate is typically observed in daytime during the summer months when the solar intensity is at its peak. While temperature affects the evapotranspiration by allowing the water to evaporate, wind and humidity rather act as limiting factors. Since air is limited in regard to how much water vapor it can hold, a higher humidity entails less evapotranspiration before the maximum relative humidity is reached. The wind could meanwhile transport the saturated air from the dank area and exchange it with less humid air which enables the evapotranspiration process to proceed.

2.1.3.2 Seasonal predictions in Sweden

The Swedish Commission on Climate and Vulnerability have with five different emission scenarios estimated the temperature increase that Sweden will experience until 2100 [4]. Two of the predictions estimated the gradual increases and were split into three periods; 2011-2040, 2041-2070 and 2071-2100, see Table 2.1. The two were RCA3-EA2 and RCA3-EB2 of which RCA-EA2 estimated a slightly higher increase in rain and temperature. It suggested a 4-7°C increase for the winter season and a 2-4°C increase for the summer season by 2100, relative to the industrial baseline. The intervals cover the entirety of Sweden while southern Sweden can expect slightly lower increase at around 5-6°C during winter by 2100. As seen in Table 2.1, the increase in temperature gradually increase for each period and significant changes can be seen already in the first period. Furthermore, the study also estimated the monthly precipitation increase in Sweden for the same periods. In 2100, it was estimated that an increase between 40 and 50mm is to be expected as the worst-case scenario with a possibility of a greater increase than 50mm. In the summer season, the interval of precipitation change lies between negative 30 to positive 40 mm per month, i.e., both a risk of more severe drought and/or increased precipitation. Like the uncertain upper limit in the winter season, an uncertainty regarding the lower limit is also present in the summer season after 2040, see Table 2.1.

Table 2.1. Worst-case scenario of temperature and precipitation increases in Sweden until 2100 [4].

	2011-2040	**2041-2070**	**2071-2100**
Average temperature increase [°C]			
RCA3-EA2 Winter	2-3	3-4	4-7
RCA3-EA2 Summer	1-2	1-3	2-4
Average increase in precipitation [mm]			
RCA3-EA2 Winter	+20-50[1]	+40-50[1]	+40-50[1]
RCA3-EA2 Summer	-30-40	-30[2]-20	-30[2]-40

[1] The increase may be greater than 50mm.
[2] The decrease may be greater than 30mm.

2.1.3.3 Extreme rainfalls in Västra Götaland

In 2013, SMHI performed a study regarding the rainfall intensity increase of 10-year rainfalls in Sweden until the year 2100 [30]. From the two statistical periods 1961-1990 and 1981-2010, SMHI formed a set of reference data regarding both precipitation and temperature increase. Six climate predictions from the two major global climate models HadCM3 and ECHAM-4 and -5 were compiled and adapted for Sweden with the regional climate model RCA3. The predictions were used to evaluate how different parts of Sweden are going to be affected in terms of intensity and duration of a 10-year rainfall. The data would, according to SMHI, suggest that predictions for other extreme rainfall events would be very similar in terms of percentage increase. The predictions were visually presented as maps of Sweden where different parts of the country are affected differently in terms of increase and standard deviation, see Appendix B. Furthermore, the predictions were split into the three different 30-year periods, namely, 2011-2040, 2041-2070, 2071-2100. The projected increase together with the standard deviation for Västra Götaland are presented in Table 2.2.

Table 2.2. Projected increase in precipitation and standard deviation in percentage points for Västra Götaland [30].

	30 min	60 min	3h	6h	12h	24h
2011-2040						
Increase [%]	10-15	5-10	0-5	0-5	0-5	0-5
Standard deviation	10-15	15-20	15-20	10-15	15-20	10-15
2041-2070						
Increase [%]	15-20	5-10	5-10	5-10	5-10	5-10
Standard deviation	10-15	5-10	5-10	5-10	10-15	10-15
2071-2100						
Increase [%]	25-30	20-25	15-20	15-20	15-20	15-20
Standard deviation	10-15	10-15	10-15	15-20	15-20	15-20

2.2 Geotechnical & hydrogeological parameters

There are many parameters which affect the behaviour of a soil. These include the mechanical properties of the soil connected to general factors such as density, grain size and void ratio. Furthermore, soil is also heavily affected by water located in and around it as well as water flowing through it. The most relevant key parameters and relationships for this study will be presented in the following section.

2.2.1 Slope stability and safety factor

Slope stability and the analysis of the subject refers to the evaluation of resisting and driving forces on a slope [31]. Slopes are both found as natural geological formations but can also be constructed to fill a purpose. A stable slope is unlikely to instantly fail and will not, under normal circumstances, succumb to sliding as long as no additional external forces affects the slope. Unstable slopes on the other hand are slopes which are on the verge of failure. There are many factors which can affect a slope's stability of which some are soil weight and distribution, slope inclination, groundwater conditions, and external forces such as precipitation or various constructions. The stability of a slope can be quantified with the use of a safety factor. A safety factor is a measurement of how likely a slope is to fail. If the factor is below 1 it would indicate that the slope will or already have failed. A higher safety factor indicates a lower probability of failure [32].

The safety factor can be calculated with different methods depending on models and software used. If the Mohr-Coulomb failure criterion is used in the software PLAXIS, a method called φ/c-reduction is used [33]. As the name suggests, the method estimates the safety factor by incrementally reducing the value of c and $\tan(\varphi)$ for a set number of steps. Where c is the cohesion parameter and φ is the friction angle, see Equation 2.3.

$$\Sigma Msf = \frac{tan\varphi_{input}}{tan\varphi_{reduced}} = \frac{c_{input}}{c_{reduced}} \qquad 2.3$$

The safety factor can thereby be defined as available strength divided by strength at failure and is equal to $\sum Msf$ where the iterative calculation converges.

2.2.1.1 Failure mechanisms

A slope failure can be classified as four different types, rotational failure, translational failure, compound failure, and wedge failure [34]. A rotational failure is common for fine-grained materials and failure typically occurs along the so called, slip surface. For homogenous materials, the shape of the slip surface is assumed to be perfectly circular hence the slope fails circularly. The rotational failure mechanism can be subdivided into three categories, base failure, toe failure, and face failure, which determines where on the slope the failure occurs, see Figure 2.3. Translational failure occurs for infinite slopes, i.e., slopes without definite boundaries, where the top layer forms a slip surface parallel to the slope. This type of failure mechanism is common for coarse-grained, layered, naturally formed slopes. Compound failures is a combination of rotational and translational failures and is characterized by a slip surface that is curved at two ends with a flat surfaced middle section. Finally, a wedge failure occurs both for finite and infinite slopes and is referred to as block failure or plane slope failure. Essentially, this type of failure emerges due to fissures, joints, or weak soil layers in a slope, or for multi-compound material slopes.

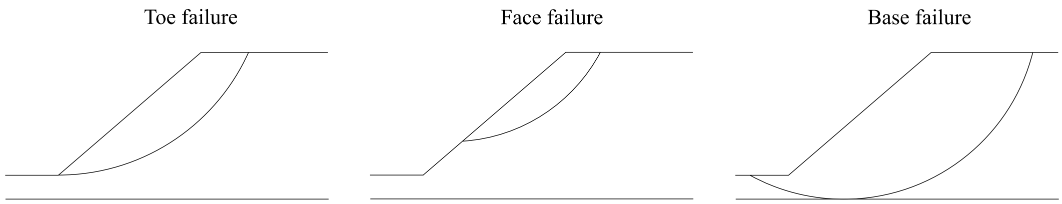

Figure 2.3. Rotational failure mechanisms for slopes.

2.2.2 Partial saturation

A soil is partially saturated when the degree of saturation is less than 1 and greater than 0. Soils are typically saturated below the phreatic line, meaning that all open pores are water-filled thus causing a positive pore water pressure. Above the phreatic level, the pores are usually unsaturated or partially saturated and does therefore generate a negative pore water pressure [35]. Negative pore water pressures are caused when water ascends in a porous material, a phenomenon known as capillary suction. The drivers for such a mechanism are cohesion i.e., the molecular attraction between molecules of the same kind, and adhesion i.e., the molecular attraction that appear between different physical bodies [36]. In soil mechanics however, cohesion is instead referred to as “the shear strength when the compressive stresses are equal to zero” [37, p.89] and should not be confused with molecular cohesion in soil physics. Capillary suction appears once the adhesion to the pore walls is greater than the cohesive forces, hence causing water surface tension and capillary rise. Materials with finer pore structure tend to experience larger capillary suction forces than more coarse-grained materials [38]. This is due to the high specific surface area of which fine-gain materials typically consist, hence having high absorption capability [39].

2.2.3 Effective stress in soil

The effective stress in a soil or porous material is the combination of factors affecting the resulting stress [40]. The simplest form of effective stress is the Terzaghi's effective stress, see Equation 2.4. In the equation, the weight of the soil multiplied by the depth equals the total stress σ from which the pore water pressure p_w for that depth is subtracted.

$$\sigma' = \sigma - p_w \qquad 2.4$$

Terzaghi's effective stress formula does however not consider to which degree a soil is saturated and the effects that the partial saturation entails. The effective stress for a partially saturated soil can be calculated with the Bishop's effective stress, see Equation 2.5. It scales the effect that the pore water pressure has on the effective stress with the matric suction coefficient χ which varies from 0 to 1. At fully unsaturated conditions it is equal to 0 while at fully saturated conditions the corresponding value is 1. In the equation, m_b is a vector which excludes the shear components of the stress and p_a is the pore air pressure.

$$\sigma' = \sigma + m_b(\chi p_w + (1-\chi)p_a) \qquad 2.5$$

The pore air pressure has a relatively small effect on the calculation compared to the pore water pressure and can essentially be set to 0 for most applications. By setting the pore air pressure to 0, the term in the equation is neglected and the simplified version, seen in Equation 2.6, can be assumed.

$$\sigma' = \sigma + m(\chi p_w) \qquad 2.6$$

2.2.4 Suction

The total suction force, S_t, of a soil is divided into two main components, matric suction S and osmotic suction π, see Equation 2.7 [35].

$$S_t = S + \pi \qquad 2.7$$

Osmotic suction refers to salinity in the pore-water which can influence the mechanical behaviour of a soil. Changes of salt content in both unsaturated and saturated soil affect the soil's shear strength and the overall volumetric properties. Relative to the matric suction, the osmotic suction constitutes a rather small influence on the soil behaviour. This does however depend on the case, and in certain situations the osmotic suction has shown to be of high relevance [41]. Nevertheless, osmotic suction is often ignored in common applications of geotechnical engineering analyses, hence the total suction can be assumed as Equation 2.8.

$$S_t = S \tag{2.8}$$

Matric suction, also known as the capillary pressure, is the difference between pore air pressure, p_a, and pore water pressure, p_w, see Equation 2.9 [40].

$$S = p_a - p_w \tag{2.9}$$

In geotechnical applications, the pore air pressure is defined to the atmospheric pressure, hence it could set to 0. The suction can therefore be expressed as the negative pore water pressure, $-p_w$, see Equation 2.10.

$$S = -p_w \tag{2.10}$$

2.2.5 Soil water characteristic curve

The soil water characteristic curve, SWCC, is used to describe the relationship between suction and the degree of saturation, also known as the effective saturation S_e, for a soil [40]. The relationship can be utilized to approximate the effective stress for a soil since the matric suction coefficient χ in Bishop's effective stress can, and often is, assumed to be equal to the effective saturation, see Equation 2.11. The matric suction coefficient is dependent on several factors of which the degree of saturation is the most prevalent, hence the assumption [35].

$$\sigma' = \sigma + m(S_e p_w) \tag{2.11}$$

There are several ways to estimate the soil water characteristic curve of a soil of which one is the Van Genuchten fitting method that the software PLAXIS utilizes. The method is in its simplest form a combination of relationships seen in Equation 2.12 and 2.13 resulting in Equation 2.14 [42], [43].

$$S_e = \frac{1}{[1+(\alpha h)^n]^m} \tag{2.12}$$

$$S_e = \frac{\theta-\theta_r}{\theta_s-\theta_r} \tag{2.13}$$

$$S_e = \theta_r + (\theta_s - \theta_r)[1 + (\alpha h)^n]^m \tag{2.14}$$

$$m = \frac{1-n}{n} \tag{2.15}$$

In Equation 2.14, α correlates to the air-entry value, h the matric potential, n the pore size distribution, and m a value related to the asymmetry of the model [44]. The value m can be expressed in term of n, see Equation 2.15. Furthermore, θ is the water content while θ_r and θ_s represents the residual and saturated water content respectively. The residual water content refers to a point of the volumetric water content where a considerable increase of matric suction does not cause significant changes of water content [45]. The saturated water content, however, refers to the volumetric water content where the soil is fully saturated, whereas the matric suction is at its minimum value [44].

SWCC curves are estimated either mathematically or by lab testing and are unique for every soil structure, yet a general form can be approximated for every soil type. The shape of the curve is primarily dependent on the pore size distribution, thus also, indirectly, the grain size distribution [46].

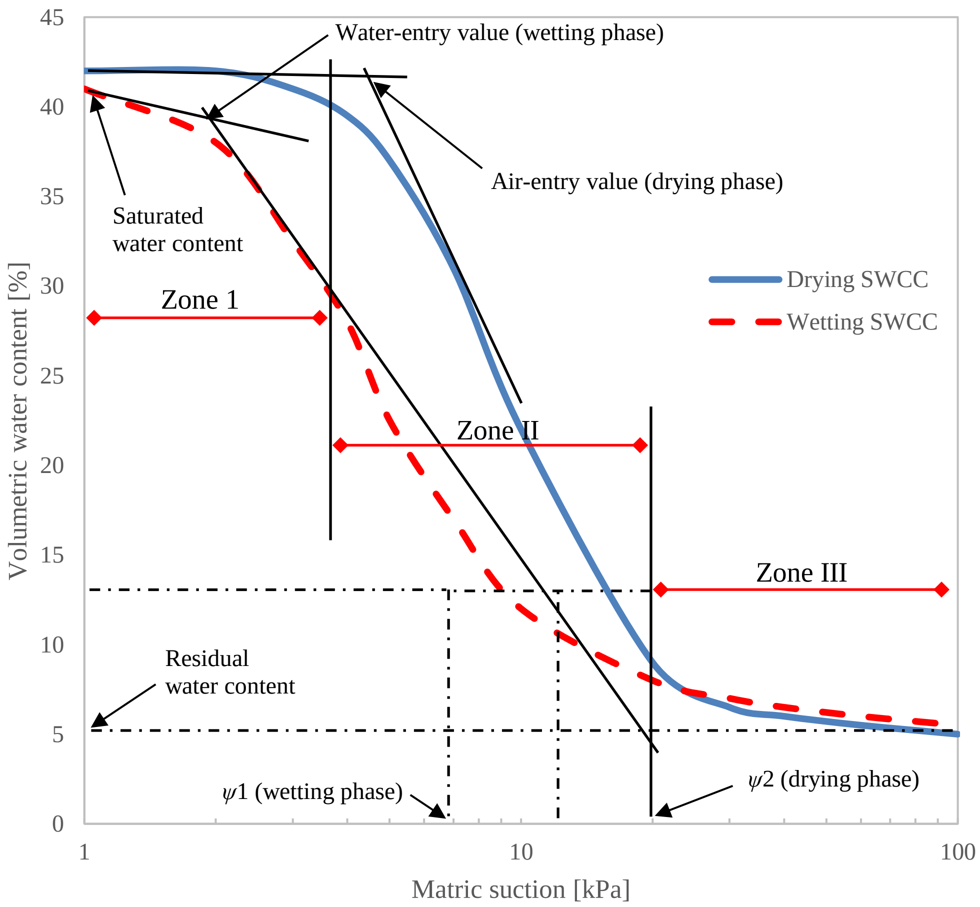

Figure 2.4. Typical SWCC for a sandy silt [44].

Figure 2.4 shows a typical relationship between matric suction and volumetric water content for a sandy soil. A wetting phase, also called adsorption, is plotted together with a drying phase, desorption. Therefore, a different suction can be obtained for a certain water content, a phenomenon known as hysteresis [44], [47].

2.2.6 Permeability curve

The permeability, also known as the hydraulic conductivity, is a measure of a soil's ability to transport water or any other liquid through the voids. A soil’s permeability is primarily dependent on the material’s particle size distribution, mineral composition, particle structure, void ratio and degree of saturation [38]. The saturation corresponds to the suction according to the soil water characteristic curve, meaning that the suction, in turn, corresponds to the permeability. A saturated soil has a higher permeability than an unsaturated soil due to otherwise air-filled voids restricting the flow of water. Once a heavy rainfall occurs entailing a reduction of the total suction, the coefficient of permeability, k_w, decreases hence making the soil more prone to infiltration [5]. Figure 2.5 portrays a typical relationship between a SWCC and the permeability function of sand and clayey silt. From the figure, it can be observed that a higher water content equals a high permeability with moderate influence of suction. However, when the soil desaturates, the coefficient of permeability decreases thus increasing the matric suction of the soil.

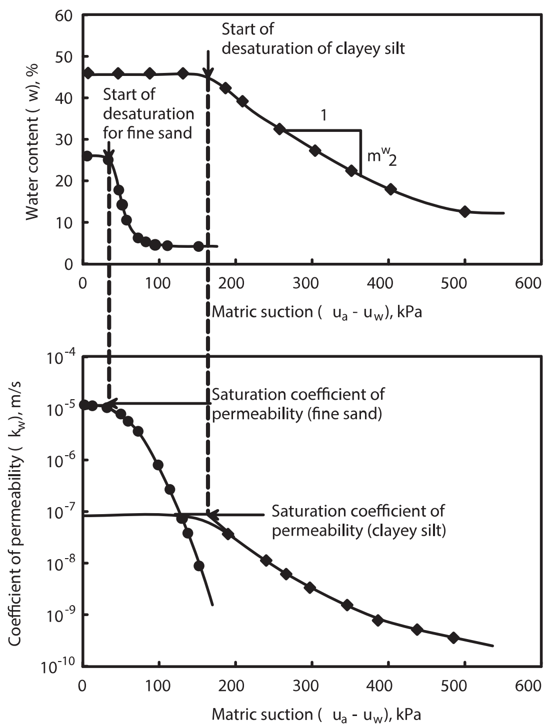

Figure 2.5. Typical relationship between SWCC and permeability function [40].

2.3 Soil modelling

There are many different models to calculate the behaviour of a soil. The different models have their strengths and weaknesses, and some are more suited for certain applications. Some of the models include the *Linear elastic model*, the *Mohr-Coulomb model*, and the *Modified Cam-Clay model* [33]. The Mohr-Coulomb model is widely used to provide a first estimate of a simulation. The model is relatively simple compared to other models and can therefore be calculated quickly to get a first assessment of the case [48]. The model is a so-called *linear elastic perfectly-plastic* model which means that an increase in strain, results in a linear increase in stress. Furthermore, since it is perfectly plastic, the model does not consider the potential recovery after a certain strain. The model is based on the Mohr-Coulomb failure criterion which explains the relationship of different stresses and the failure of a soil.

2.4 Finite element method

The finite element method, also known as FEM, is a numerical method that aims to simulate a complex scenario with a determined number of elements [49]. In the case of soil modelling, FEM can be used to solve scenarios which otherwise would be very complex or even impossible. The concept is that a geometry is split into a mesh of elements which are either areas or volumes depending on if the case is two-dimensional or three-dimensional. These elements can be given certain properties to how they interact with each other. The accuracy of the simulation is to a certain degree correlated to the refinement of the mesh, i.e., the number of elements [49]. The elements can have different shapes and different number of nodes, which are the points where elements connect.

3
Location

The following chapter describes the location at which the simulations are based. Important geological and hydrological conditions will be presented. Additional focus will be directed to the studied section and the geology in close proximity.

3.1 Hjärtum

Hjärtum is a small urban area in the Lilla Edet municipality and is located at the west side of the Göta älv river, roughly 54km north of Gothenburg. In the area is an uninhabited land slot of approximately 500 by 300 meters, locally called Sörängen. The area is partly consisting of a relatively steep natural slope which is deemed critical in terms of safety factor. Sörängen is bound in the east by Göta älv and to the north by the stream Sollumsån which connects to Göta älv. To the south and west, the investigated area ends where the land is less steep, and failure is less likely. South of the slope are earlier signs of slope failures which have formed the current geology thus the present stability. One of the precautions that have been applied is an erosion protection in the form of a layer of blasted stone along the shore of Göta älv. The road Kungälvsvägen, also known as Road 2025, runs through the western part of the investigated area at the relatively flat soil, see Appendix A.

Göta älv is Sweden's largest river in terms of run-off area and water flow, supplying hundreds of thousands of inhabitants along the river with drinking water [50]. Additionally, the river is a key provider of water for the operation of agricultural and industrial services while at the same time being a meaningful fairway for marine traffic [51]. Göta älv is in the western part of Sweden, originating from Lake Vänern and flowing out in Kattegat. In Kungälv, located approximately 20 km north of Gothenburg, the river is separated into two flows. One stream flow north of Hisingen Island, known as Nordre älv, which constitutes a major part of the total water volume. A smaller part continues south and flow out via Gothenburg to the archipelago and eventually Kattegat. There are 58 flood gates in the river that regulates flow to both keep the river from overflowing and to keep the flow at an adequate rate.

The company SWECO performed an investigation of the area in 2019 on behalf of the Swedish Geological Institute, SGI. For their investigation, several boreholes were drilled in order to determine the soil composition and soil properties. There are five separate investigated sections for SWECO's study, three of them, 25/730V, 25/890V and 26/100V are directed towards Göta älv at the east. The other two sections, 25/670VRS1 and 25/670VRS2 are examining the slope stability on the northern part of the site, facing towards Sollumsån. The section examined in this study is the 26/100V section, the southernmost located. In proximity to this are boreholes 19SW04 to 19SW07 as well as 19SW10 located just south of the section, see Figure 3.1.

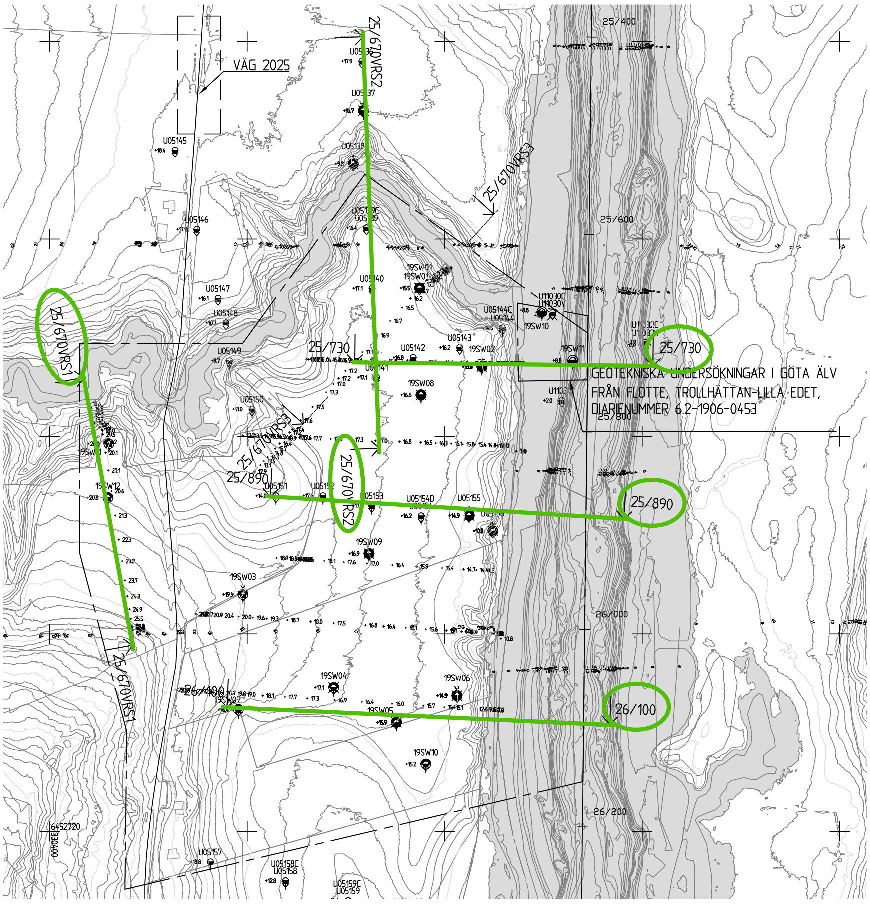

Figure 3.1. Map showing cross sections in green for the investigated area.

3.1.1 Topography

The examined slope in Hjärtum is characterized predominantly by farmland which constitutes the land east of the road. West of the road is an unused, natural soil structure. The topography is varying slightly for each section. Generally, however, the road is placed at +21-meter elevation and the slope crown at +15-meter elevation making the inclination from these points less than 2°. From the slope crown there is a significantly steeper part to the edge of the shore at a +8-meter elevation, thus an inclination of roughly 26.6°. In the river, there is a 20-meter-deep underwater slope, declining steeply towards the furrow of the river.

3.1.2 Stratigraphy

The stratigraphy at the location of the slope and the area around the slope is similar to most soil conditions found along Göta älv [52]. It is mostly consisting of a silty clay, slightly varying in thickness between the river and upland. At the connection to Göta älv, the clay layer exceeds 50m of depth. Above the clay, closest to the surface, is a dry crust which in the investigation was assumed to be cracked and at some locations, halfway filled with water. The friction angle was conservatively assumed to be 30° and the dry crust was assumed to have no shear strength due to the cracks. Quick clay has been identified at one of the middle locations of the site, namely at the borehole 19SW09, north of the investigated section, see Figure 3.1. The quick clay was found between the depths 16m and 25.5m and has a sensitivity ranging between 20 and 25 which indicates a normally sensitive clay. Other than the quick clay, the stratigraphy of the area is relatively consistent. Between the different boreholes, the amount of silt and other grain sizes varies slightly which does affect certain parameters to some extent. Inland, the clay is normally consolidated to slightly overconsolidated while below Göta älv, it is overconsolidated. Below the clay is a friction soil, also called a cohesion soil, with a shear strength of 0 and a friction angle of 38°.

3.1.3 Geotechnical parameters

Several conducted measurements techniques were used to derive crucial geotechnical parameters for the slope stability analysis. For the undrained shear strength derivation, a series of test results from the different methods were compiled and a trend line was best fitted to find a representative value. The direct shear test, vane shear test and triaxial test weighed heavier than the rest and were deemed most representative for the parameter choice. CPT tests were primarily used to determine the increasing shear strength at the greatest depths. Additional fall cone test was performed, however, results from this method does generally indicate lower shear strength with depth than the rest, hence results below 20 meters from this method have been neglected. Measurements have also been conducted to determine the undrained shear strength in the river. Due to missing support of direct triaxial test and direct shear test, the undrained shear strength was represented from fall cone test, vane shear test, CPT and CRS. For the drained shear strength in the friction soil, empirical assessments determined the input parameters and cover the entirety of the site. The clay indicates a slight anisotropic condition with the relationship between vertical and horizontal stress, K_0, varying from 0.55 to 0.7.

3.1.4 Hydrogeological conditions

The water level in Göta älv is regulated downstream by a nearby floodgate located in Lilla Edet. Once the floodgate is closed, the water level reaches up to 7.6 meters. On the contrary, a water level of 6.6 meters is obtained while the floodgate is open. Measured pore pressures at the site indicate a groundwater table located 1-2 meters below surface level. From there, hydrostatic conditions apply i.e., the pore pressure increases linearly with the depth.

The clay indicates a homogeneous soil structure, hence water transport through cracks and similar soil abnormalities could be neglected. The pore pressure conditions are governed by the more permeable layers i.e., the dry crust and erosion protection with permeabilities at 1.4E-4 m/day and 863 m/day, respectively. The permeability for the clay layers has been measured at four depths 6m, 10m, 25m and 35m at borehole 19SW06. As Table 3.1 suggests, the permeability decreases with depth. The hydrogeological properties for the clay layers at the site correspond to a typical Swedish clay [53].

Table 3.1. Hydrogeological conditions for borehole 19SW06 derived from CRS testing.

Depth	Permeability [m/day]
6m	1.30E-4
10m	1.12E-4
25m	1.04E-4
35m	4.92E-5

3.1.5 Section 26/100V

The investigated section 26/100V indicates a similar stratigraphy as the rest of the site with a top layer of organic surface soil followed by a dry crust and lastly a thick layer of homogeneous, partly silty, clay. Beneath the clay, at the western part of the section, is a thin layer of friction soil, see Figure 3.2. The thickest layer of clay in the section is observed at the slope crown, adjacent to borehole 19SW06, with a thickness of 47 meters. From there, the soil depth declines to the west where the clay thickness is 5 meters at point 19SW07. The thickness of the friction soil is declining towards the river and is around 1-meter-thick east by the slope crown. On the contrary, the thickness of the friction soil is 6m at the western part of the section. Laboratory tests suggest a density generally varying between 1.6-1.7 ton/m^3. The water content in the clay ranges between 60%-75% with the highest values at the bottom of the layers. The sensitivity is 15-25 in borehole 19SW06 as well as in the upper part of 19SW05. At the depths 24-30 meters, the sensitivity is slightly higher at 38-66 for 19SW05. The shear strength in remoulded samples indicates no signs of quick clay for 19SW05. However, the CPTR-measurements indicate quick clay at the flatter, western, part of the section, namely at borehole 19SW04 and 19SW07. Pore pressures have been recorded at four levels: 6m, 11m, 16m, and 21m at borehole 19SW05. For 19SW06, piezometers have been installed to record pore pressures at six levels, 5m, 10m, 15m, 20m, 25m, and 29.6m, below the surface. As for the rest of the site, hydrostatic conditions apply with the groundwater table located 1 meter below the surface. The pore pressure trend chosen for SWECO’s study is presented in Figure 3.3.

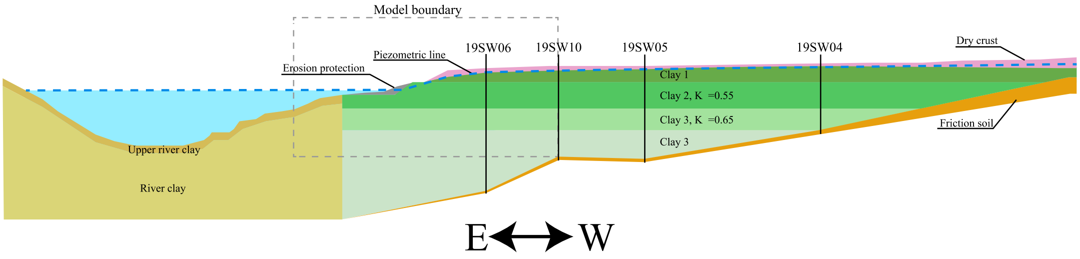

Figure 3.2. Cross-section with stratigraphy for section 26/100V.

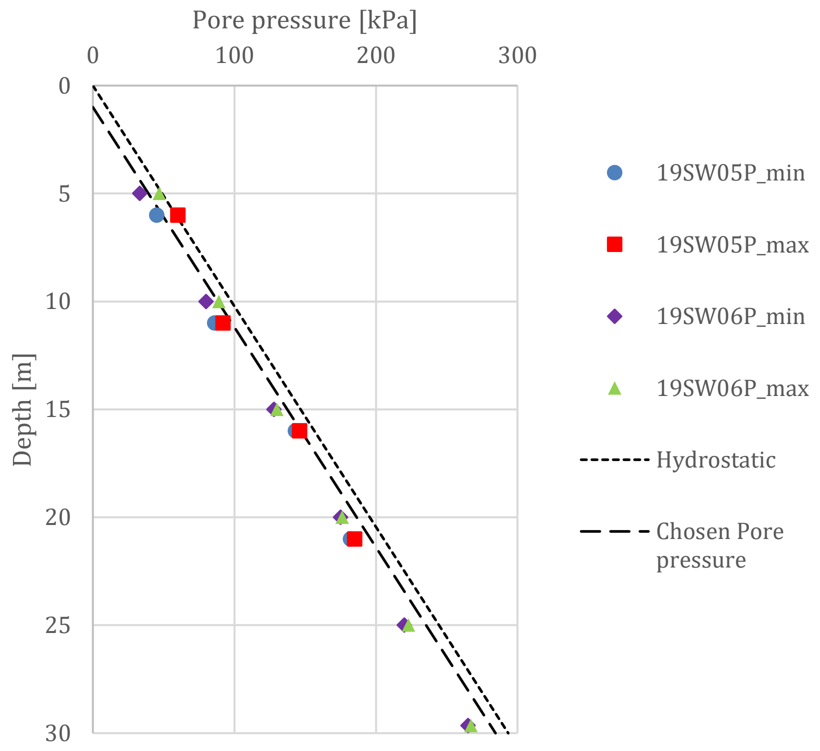

Figure 3.3. Measured pore pressures with estimated trend.

The input parameters unit weight, anisotropy, and friction angle for the soil layers are presented in Table 3.2.

Table 3.2. Soil properties for the clay layers on land.

Definition	Unit Weight [kN/m^3]	Anisotropy [-]	Friction angle [°]
Dry crust	17.0	0.5	30
Clay 1	16.2	0.6	30
Clay 2a	16.5	0.55	30
Clay 2b	16.5	0.65	30
Clay 3	16.1	0.65	30
Erosion protection	20.0	0.33	42

4
Method

This chapter will present the methods of the study and explain how the results were derived. The different tools used during the investigation will be introduced and explained.

4.1 Precipitation predictions

To determine how future years may present themselves in terms of precipitation, the predictions made by SMHI and the Swedish Commission on Climate and Vulnerability, were utilized, see 2.1.3.2. Together with this, two different scenarios were established to evaluate how different types of rainfalls affect the stability of a natural slope. The reference period 1961-2010 was used to identify the worst-case scenarios in Västra Götaland from the time-period which the predictions are based upon. The first scenario being the month with the most extreme single rainfall event and the second being the most total precipitation in one month.

The weather station Göteborg A was chosen to represent the area of the study due to it being one of the closest stations to the investigated site with available hourly data. There are several weather stations which are closer to the studied site, these are, however, either non-active, do not record hourly data, or does not cover the reference period. A disclaimer is that there is a missing dataset at station Göteborg A between 1977-1995 when the station had to be shut down (T. Carlund, personal communication, March 10, 2022). Additional interruptions of data recording have occurred during the reference period, however never longer than nine months. Nonetheless, a substitutional measurement station located in Säve, Gothenburg recorded data during the missing periods. It was assumed that Säve and Göteborg A recorded close to identical values during that period, hence data from Säve have been used to complement the missing data for Göteborg A between 1977-1995 as well as the short interruptions. Furthermore, it was found favorable to utilize data at Göteborg A after 1995 since that was when an hourly measurement started to be logged. The hourly precipitation would entail a much more accurate simulation in the later stages of the study. That being said, data from earlier than 1995 was not ignored but in the case of similar data, the one from after 1995 would be selected to obtain more accurate results.

The reoccurrence time for the extreme rainfalls was determined with Dahlström's formula to put the intensity of the rainfalls into perspective. The study was restricted to identify rainfalls with a reoccurrence time larger than 1 year. Particularly small precipitation volumes, at or below 0.1mm, were neglected for extreme rainfalls. This would mean that the calculation of the reoccurrence time only considered the hours of an extreme rainfall where the rain intensity exceeded 0.1mm. The reoccurrence times were obtained as months and subsequently rounded to years as the closest integer.

The negative discharge considered for the study was obtained from the evaluation of evapotranspiration by Eriksson which considered time of year and location in Sweden [54]. The investigation was performed for the period 1961 to 1978 which corresponds to the beginning of the reference period for the precipitation prognosis in this study. Furthermore, it has been concluded that climate change will inevitably affect the evapotranspiration [55]. By 2049, a maximum increase of about 10% could be seen in August for climates resembling Iran. However, due to the lack of similar studies for Sweden and the small effect compared to the increase in precipitation, future prognoses for evapotranspiration were neglected. The values are thus relative to the average evapotranspiration to the area around Västra Götaland between 1961 and 1978 for all the investigated future years.

4.1.1 Scenario 1: Increase of extreme rainfall events

The study performed by SMHI in 2013 [30] regarding the intensity of 10-year rainfalls was, in this study, used as a basis to evaluate extreme rainfall events until the year 2100. It was assumed that the increase was applicable on all rainfall events which could be classified as extreme. Since the increases in Table 2.2 was presented as intervals, upper and lower limits were obtained. The average standard deviation was added to the upper limit and subtracted from the lower limit from which the percentual increases for each time-period and duration were obtained.

To obtain results for the worst-case scenario, the month with the single most extreme rainfall event in Västra Götaland from the reference period had to be identified. The daily precipitation measurements from SMHI’s weather stations Göteborg A and Säve was sorted by the day with the highest amount of precipitation. The hourly precipitation data from the same station was then analyzed to determine a more exact duration and intensity. The duration of which the rainfall occurred was compared to Table 2.2 and eventually multiplied by the percentual increase for the corresponding duration and time-period.

4.1.2 Scenario 2: Monthly increase in precipitation

The seasonal increase in precipitation has been evaluated in accordance to how climate change will affect temperature and precipitation for the different months of a year. The Swedish Commission on Climate and Vulnerability estimated, with several commonly used climate models, that temperature will increase more for the winter season than for the summer season [4]. For the study, October to March was defined as the winter months of the year while April to September was defined as the summer months. A greater increase in temperature in winter would indicate a significant precipitation increase while the summer season may experience, either less precipitation or an increase of precipitation. As the upper limits of the precipitation are just defined as higher than 50mm for the winter months, an extrapolation had to be made. According to the Clausius Clapeyron relationship between temperature and precipitation, a 1°C increase roughly entails a 7% increase of atmospheric water vapor content. It was assumed for the study that every rainfall would be affected equally in terms of precipitation volume and not only the most extreme rainfalls. The upper limit of the increase in precipitation each winter month was therefore extrapolated to correlate to the increase in temperature. For the summer months, upper limit was divided directly with the number of rainfalls since the upper limit was not as uncertain.

To evaluate the worst-case of seasonal increase for the periods 2011-2040, 2041-2070, and 2071-2100, the rainiest month was selected from the reference period 1961-2010. The upper limit of the monthly extrapolated increase was then divided by the number of rainfalls and added to the days when a rainfall occurred. The reason that the upper limit was chosen was to acquire the worst-case scenario, similar to earlier assumptions. It was also assumed that an increase in precipitation would not affect the number of rainfalls but rather the intensity of existing ones. Unlike the method of adding evenly distributed monthly precipitation, the most extreme rainfall identified during the month, i.e., reoccurrence times larger than 1 year, were corrected with the method from scenario 1.

4.2 Soil simulation

For the study, the software PLAXIS 2D was utilized to model the slope with a finite element method. A plain-strain model with 15-noded elements was used throughout the entire study. Initially, the geometry of the model was exported from SWECO’s provided Geostudio SLOPE/W model to PLAXIS, see Figure 3.2. To simplify the simulation and lower the calculation time, the model was cut to only include the steepest part of the slope where the failure is most probable to occur, indicated as a dashed line in Figure 3.2. The material model used in the calculation was the Mohr-Coulomb model and the drainage type was set to drained. The flow boundaries were set to closed for the right and left boundaries while the upper and lower were set to open. On the contrary, the right and left boundaries were locked in horizontal direction in terms of deformations while the lower boundary was locked in both directions and the upper boundary was left open. The groundwater table and water level in the river utilized in the model by SWECO corresponds to the minimum level in Göta älv at this location and was not modified. To acquire accurate results, it was determined that an average mesh element size of around 1m was desired. The mesh was subsequently refined incrementally until the results converged.

The five soil layers in the model were defined primarily from the available parameters in the study by SWECO and the main parameters can be found in Table 3.2. Parameters not specifically defined in the study was left at the default value in PLAXIS. The friction angle and the effective cohesion were obtained through the available active undrained triaxial tests, according to Appendix C. Certain unknown parameters were estimated by analysing similar soil compositions with comparable conditions. The clay was deemed normally to slightly over-consolidated, thus Poisson's ratio was set to 0.2 for all soil layers [56]. Furthermore, since the focus of the study does not include deformations, the stiffness modulus E', was deemed adequately accurate at 10 MPa for every layer which corresponds to a typical value for silty clay. The effective cohesion for the dry crust and erosion protection are in practicality zero, although a value of 0.5 was assigned for numerical stability. Furthermore, the permeability for the same materials were compared and estimated to typical values of such materials. The permeability for the clay layers were derived by SWECO, however, the permeability for the dry crust was set to a standardized value corresponding to 1.4E-3 m/day. For the erosion protection, the permeability was set to 863 m/day.

4.2.1 Infiltration

To define the infiltration for the model, the behaviour of the soil boundaries above the water level in the river was set to infiltration. Furthermore, the time dependency was set to constant for each day of the month in order to assign the daily precipitation volume. The precipitation volume for each day, reference values, and projected values, were subtracted with the assumed constant evapotranspiration for August and October, respectively. In order to determine the suction behaviour relative to the rain infiltration, a user-defined Van Genuchten soil water characteristic curve was defined. Since no prior examination of the SWCC had been made for the site, a SWCC for a similar soil type was utilized. The MatLab curve fitting tool was used to determine the parameters θ_r, θ_s, α and n which PLAXIS requires to define the SWCC. These values were applied to the layers which are entirely or partially above the ground water table. Since the layers below the ground water table would not be subject to the effect of suction, these were defined as saturated.

4.2.2 Phases

For the staged construction, the calculation type of the initial phase was set to *gravity loading* due to the presence of non-horizontal layers. Furthermore, the pore pressure calculation type was defined as *phreatic*. To simulate a full month of precipitation, 31 days of fully coupled flow deformation analysis were conducted. Together with each day, an additional phase was added to determine the safety factor for each consecutive day. The safety calculations were based on a φ/c' reduction using incremental multiplier as the loading type. By iterating the φ/c' reduction, the value ultimately converges, therefore the number of steps was set high enough to obtain the most accurate result.

5
Results

In the following chapter, future precipitation prognoses will be provided for each of the examined time periods. Furthermore, the effect that the increased precipitation has on the slope in Hjärtum will be presented in terms of and safety factor, suction and slip surface.

5.1 Precipitation conditions

The following sections presents results from precipitation scenario 1 and 2 for the reference years together with future time-periods. The month with the most extreme single rainfall was identified in August 1997. On the other hand, the rainiest month was found to be October 2006. However, it should be noted that this month was not the most rain dense month for the weather station *Garn* closest to Lilla Edet. In fact, the historically rainiest month for the location did slightly exceed the chosen month in Gothenburg. Nevertheless, as the method suggested, this dataset was substituted with hourly available data from Gothenburg during October 2006. The single most extreme rainfall between the locations did however differ more significantly, although deemed representative for the study.

5.1.1 Scenario 1: Extreme rainfall identification and future prediction

The results from the future precipitation predictions are presented in Table 5.1. From the table it can be observed that the most affected rainfall type, in terms of increase, is the short duration rainfalls, with the 30-min duration rainfall being the most severe of them. Moreover, a negative change is observed at several time scenarios and durations which would indicate a reduction of certain types of extreme rainfall events. The negative factors were obtained when the standard deviation exceeded the lower limit of the interval on several occasions. For the short-term projection, 2011-2040, the most volatile of duration is observed at 3h and 12h, where the interval ranges 40 percentage points. For 2041-2071, the negative change has reduced, relative 2011-2040, while the maximum increase is similar. The long-term prediction, 2071-2100, only indicates a minimal possibility of decrease for extreme rainfall events for 6h, 12h and 24h. Additionally, the maximum increase suggests a trend of significantly more intense rainfall for all durations.

Table 5.1. Percentage of increase for extreme rainfall events with different durations.

	30min	1h	3h	6h	12h	24h
2011-2040						
Minimum [%]	-2.5	-12.5	-17.5	-12.5	-17.5	-12.5
Maximum [%]	27.5	27.5	22.5	17.5	22.5	17.5
2041-2070						
Minimum [%]	2.5	-2.5	-2.5	-2.5	-7.5	-7.5
Maximum [%]	32.5	17.5	17.5	17.5	22.5	22.5
2071-2100						
Minimum [%]	12.5	7.5	2.5	-2.5	-2.5	-2.5
Maximum [%]	42.5	37.5	32.5	37.5	37.5	37.5

The day with the single most intense rainfall event during the studied period 1961-2010 was identified on the 26th of August 1997 where 85.7mm rain fell over a 13-hour period. The intense rainfall on the 26th ended a three-day long period of significant precipitation ultimately adding up to a total amount of 140.1mm. Figure 5.1 presents the increased volume for each time-period together with the reference value 85.7mm from 1997. According to Dahlström's method, the historically intense rainfall corresponds to a rainfall with a reoccurrence time of 67 years, based on a 13-hour duration, see Figure 5.2. While 2011-2040 and 2041-2070 indicate an identical increase at 22.5% from the reference value in 1997, the long-term projection suggests a 37.5% increase. The predicted precipitation of the extreme rainfall event for 2011-2040 and 2041-2070 are identical and corresponds to a rainfall with a reoccurrence time of 112 years. Moreover, for 2071-2100, the predicted intensity corresponds to a reoccurrence time of 159 years. These reoccurrence times are relative to present conditions according to Dahlström's formula.

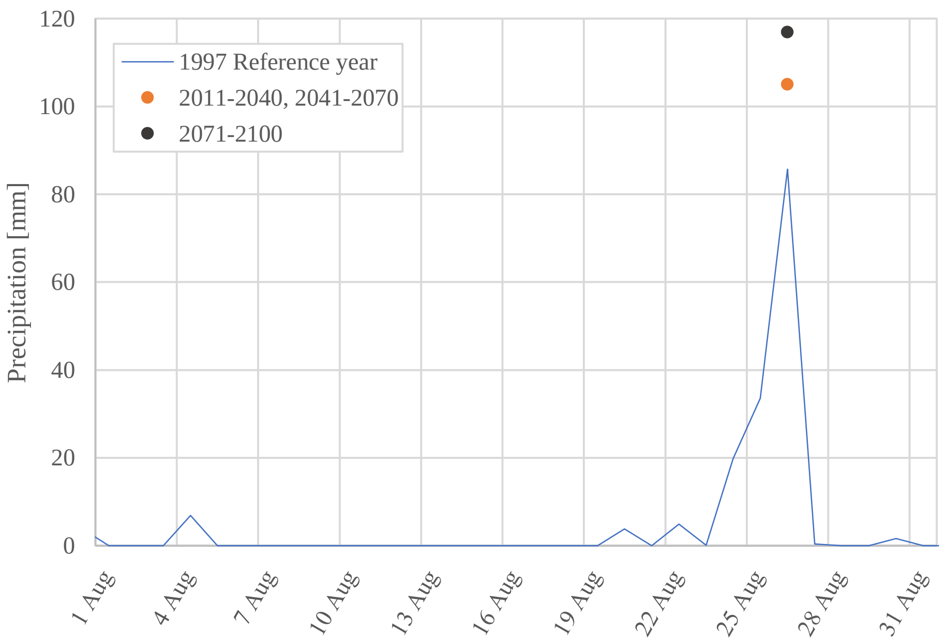

Figure 5.1. Scenario 1: Predictions of the month with the single most extreme rainfall event in Västra Götaland.

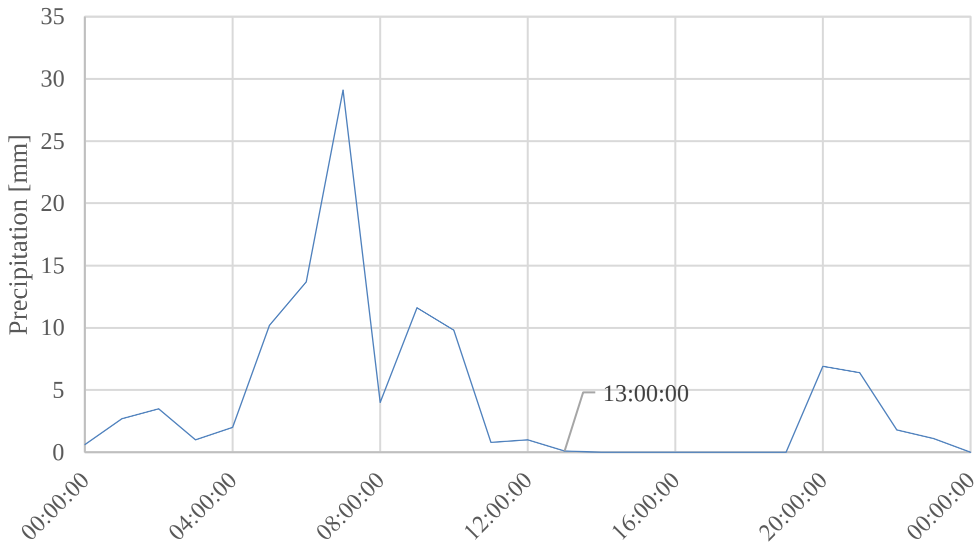

Figure 5.2. Hourly precipitation data for August 26th, 1997.

5.1.2 Scenario 2: Monthly precipitation increase

Table 5.2 shows the predicted seasonal precipitation increase with extrapolation for the future scenarios. By winter, a higher amount of precipitation can be expected for every period. However, in summertime, the range of the interval is greater than for the winter months, indicating that there is a higher uncertainty for that season. In the summer, the climate change will appear as, either a reduction or an increase of precipitation. For the first time-period, 2011-2040, an increase of 20mm to 50mm can be expected for the winter months. For 2041-2070, the corresponding values are 40mm to 53.5mm. The largest increase can be expected for the time-period 2071-2100, with a monthly increase between 40mm and 65.5mm, see Table 5.2. Commonly for all scenarios is that a reduction of precipitation might become a reality for future summer months. However, an increase of precipitation can also be expected with the short and long-term projection being the most severe of them, see Table 5.2.

Table 5.2. Extrapolation of precipitation increase for winter and summer for each scenario, presented as monthly impact.

	Extrapolated precipitation increase interval [mm]
2011-2040	
Winter	20-50
Summer	-30-40
2041-2070	
Winter	40-53.5
Summer	-30-20
2071-2100	
Winter	40-65.5
Summer	-30-40

The most intense rainfall during the month was identified on the 28th of October where 43.1mm fell over the day, see Figure 5.3. According to Dahlström's method, the reoccurrence time for the extreme rainfall would correspond to 3 years. With the correction for extreme rainfall, following the methodology from scenario 1, the reoccurrence time for 2011-2040 and 2041-2070 would be 7 years. For the time-period 2071-2100 however, the reoccurrence time is 12 years. Commonly for all time periods is that the reoccurrence times are greater than for the reference year. No other rainfalls during October 2006 had a reoccurrence time greater than 1 year, thus no correction has been made. The values are calculated according to Dahlström's formula with present conditions.

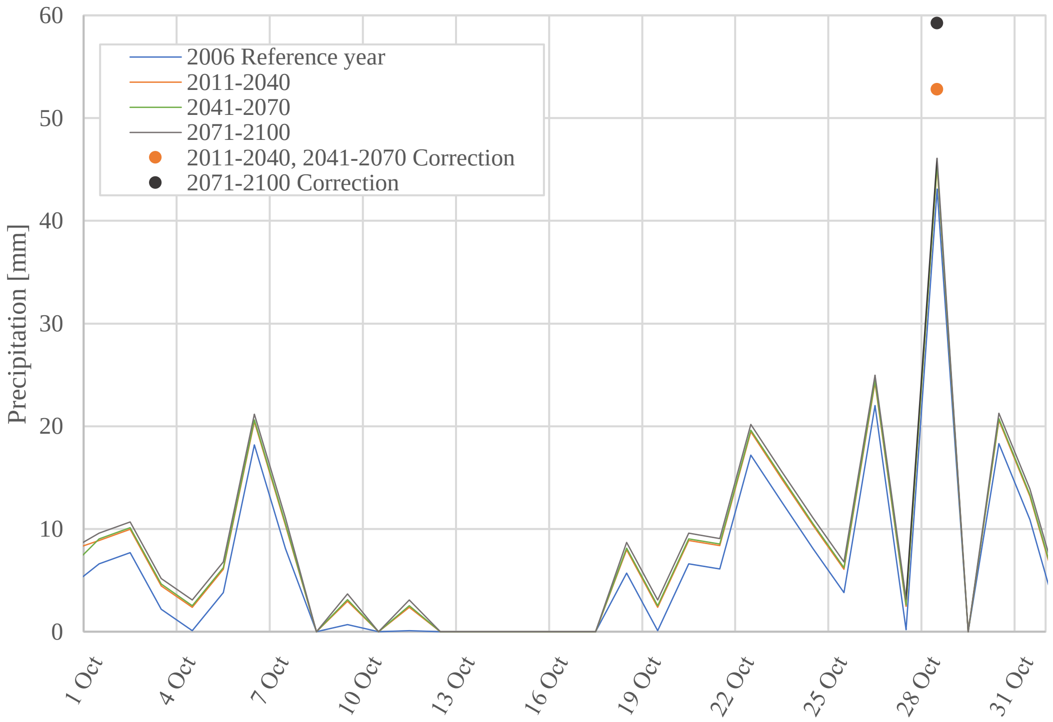

Figure 5.3. Scenario 2: Rainfall predictions with monthly precipitation increase and extreme rainfall correction applied.

Figure 5.3 illustrates the reference month, October, in 2006 together with predicted monthly precipitation increase and correction for extreme rainfalls. Table 5.3 presents the number of rainfalls and the corresponding precipitation increase for each rainfall and time-period. The total precipitation volume during the month amounted to 200mm, making it the rainiest month during the reference period 1961-2010. The projection for 2011-2040, with monthly added precipitation and correction for the extreme rainfall, results in a total precipitation volume of 259.6 mm. Thus a 30% increase from the reference value, see Table 5.4. The same value is 263.2mm for 2041-2070, making it roughly 32% larger than the reference month. With the added increase for the 2071-2100 prediction, a total precipitation volume of 281.8mm could be expected, an increase of almost 41%.

Table 5.3. Number of rainfalls and precipitation increase for each rainfall.

	Number of rainfalls	**2011-2040 [mm]**	**2041-2070 [mm]**	**2071-2100 [mm]**
Oct	22	2.27	2.43	2.98

Table 5.4. Scenario 2: Extreme rainfall event with corrected increase for the extreme rainfall and the total monthly precipitation.

	28 Oct [mm]	**Precipitation [mm]**
Reference	43.1	200.0
2011-2040	52.8	259.6
2041-2070	52.8	263.2
2071-2100	59.3	281.8

5.2 PLAXIS stability analysis

The following sections presents the safety factor, suction, and slip surfaces for the slope in Hjärtum and for the two precipitation scenarios. Two nodes are chosen to present the suction at two different locations, named point A and point B, see Figure 5.4. Point A is located roughly 0.8m below the surface and is the last point where suction is present during intense rainfall scenarios. Point B on the other hand is located at the crown of the slope and is the first place where suction disappears during precipitation. Furthermore, it is also the most prominent location for the recovery of suction. The parameters derived for the study are presented in Appendix C. These include Stiffness, friction angle, effective cohesion, and the SWCC.

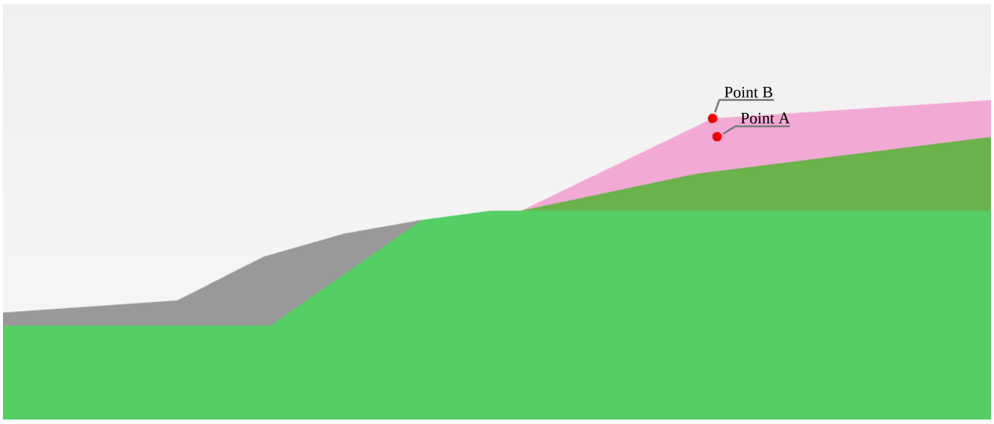

Figure 5.4. Selected nodes for the examination of suction.

5.2.1 Scenario 1

Figure 5.5 presents the precipitation for the reference year 1997 together with the future scenarios and the corresponding safety factor for each case. Note that the rainfalls for the safety calculations are subtracted with a constant evapotranspiration of 3.226mm to simulate the effect of negative discharge. From the figure it can be observed that the safety factor for the initial day equals 1.636. When a rainfall of 6.9mm occurred during the 4th of August, the safety factor reduced to 1.611. The rainfall was followed by a sequence of no rain until the 20th when a 3.8mm rain fell, ultimately reducing the safety factor to 1.602. The intense rainfall sequence for the month began on the 22nd with the most extreme rainfall striking the 26th. As can be seen in Figure 5.5, the safety factor is reduced in correlation to the rain event. The lowest safety factor for all scenarios, including the reference year, is observed on the rainiest day and equals to 1.252 which would indicate no slope failure. After two days, as the heavy and relatively long-lasting rain dissipates, the safety factor recovers to its initial state.

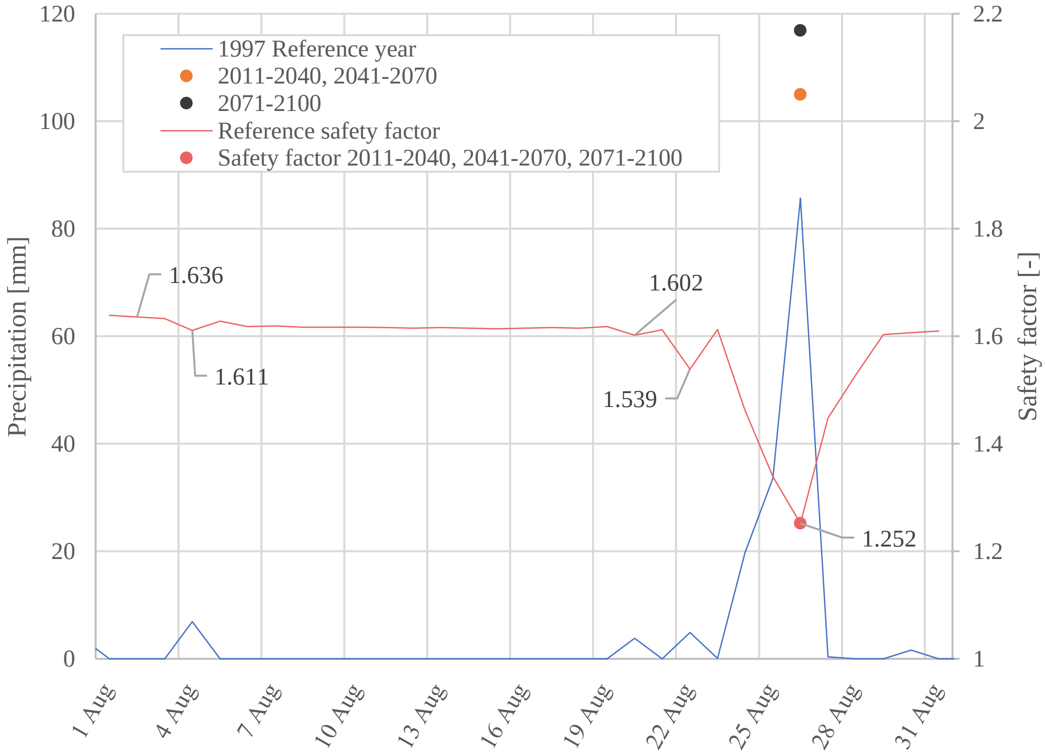

Figure 5.5. Safety factor for scenario 1, including the future scenarios, together with the precipitation for each respective case.

From Figure 5.6 it can be observed that the suction behavior differs significantly between point A and point B. For point A, a negative trend is observed from the first day until the heaviest rainfall occurred on the 26th of August, where the suction eventually recovers. A steeper inclination of the suction is observed once a rainfall occurs, meaning that there is a clear correlation between rainfalls and rate of suction. The lowest suction obtained in point A is 0.6796 kPa which correlates to when the safety factor is at its minimum. From the 26th and forward, the suction increases which ultimately raises the safety factor. For point B, a rapid reduction occurs on the four first days after which the suction stabilizes. The suction then holds a constant value until the 20th where the suction completely dissipates. As can be seen in Figure 5.6, the suction recovers instantly when a rain-free day occur and is, on the contrary, kept at zero when consecutive days of rain takes place. After the lengthy rain event, lasting between the 24th and the 27th, the suction in point B stabilizes at 10.2 kPa. The suction in point A is, during the investigated month, approaching an equilibrium between 6.72kPa on the 19th and 4.44kPa on the 31st.

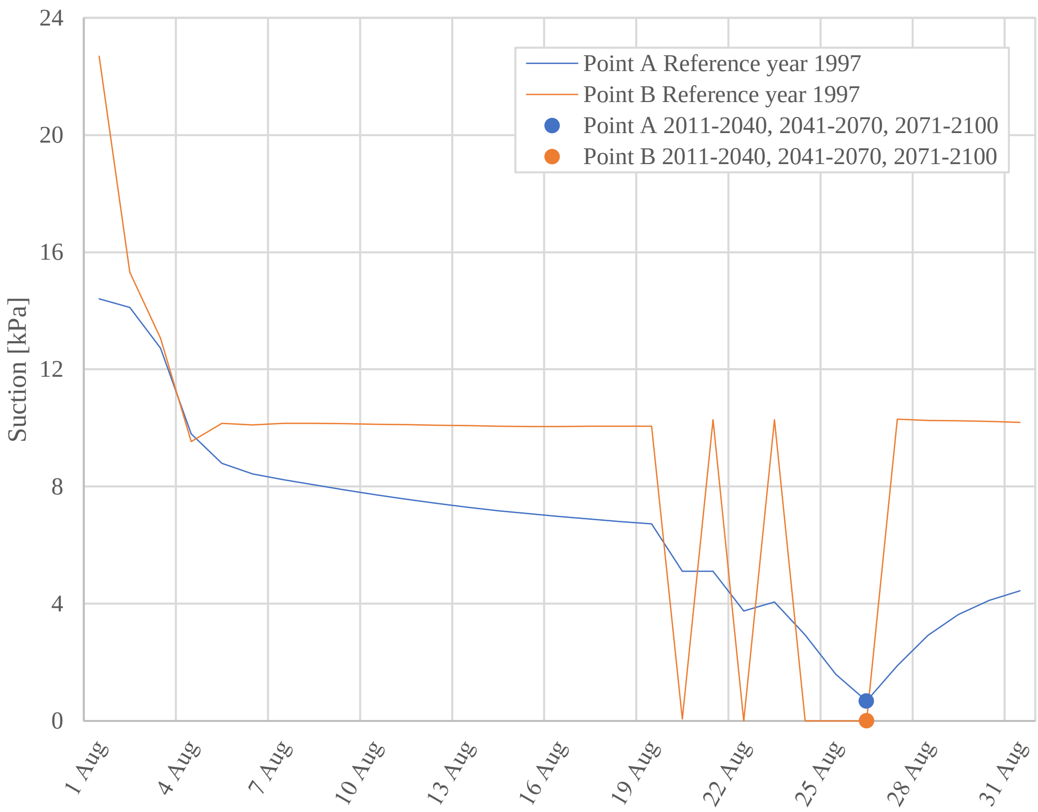

Figure 5.6. The suction for point A and point B during precipitation conditions in scenario 1.

5.2.2 Scenario 2

Figure 5.7 to Figure 5.10 presents the safety factor together with the precipitation for the reference year and future scenarios. From the figures it can be observed that the safety factor is identical between the future scenarios, even though the precipitation volume differs. However, a generally lower safety factor is obtained for the future scenarios compared to the reference year. The lowest safety factor during the month is obtained on the 31st of October at the end of a rainy sequence where it rained 12 out of 13 days. Interestingly, a safety factor below 1 is observed already on the 27th which would indicate that the slope already is on the verge of failure. Despite a series of relatively extreme rainfalls, the lowest safety factor is obtained when the most consecutive rainfalls occur. As presented in Figure 5.7, the small rainfalls for the reference year are most affected in terms of safety factor when compared to the future scenarios.

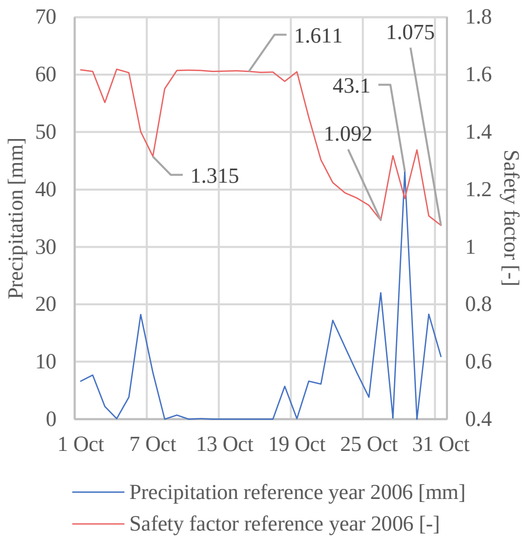

Figure 5.7. Safety factor for the reference year 2006 in scenario 2 together with the precipitation.

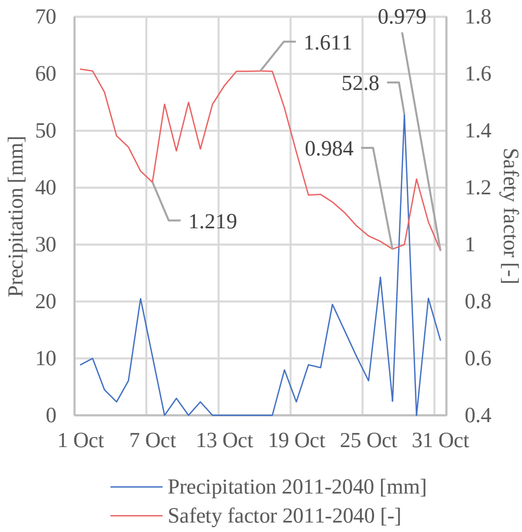

Figure 5.8. Safety factor for 2011-2040 in scenario 2 together with the precipitation.

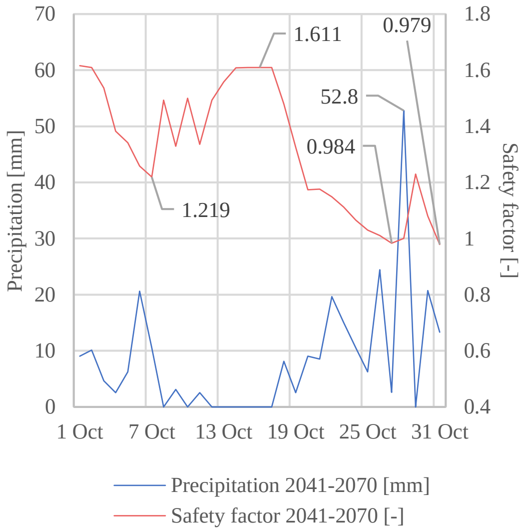

Figure 5.9. Safety factor for 2041-2070 in scenario 2 together with the precipitation.

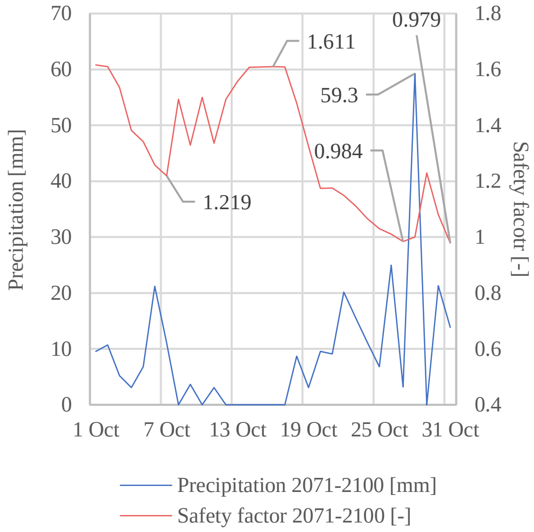

Figure 5.10. Safety factor for 2071-2100 in scenario 2 together with the precipitation.

For the examined future years, a safety factor lower than the reference year 2006 is observed for all days of the month except October 3rd where a marginally higher value is noticed, see Figure 5.11. The safety factors for all the future cases are identical and are thus represented by a single line. At all dates where the safety factor differs more than marginally, an almost negligibly small rainfall below 1mm can be observed for the reference year, see Figure 5.3. The first being the 4th of October where a 0.1mm rainfall occurred, for tabulated values see Appendix D. The same rainfall corresponded to

2.37mm, 2.53mm, and 3.08mm for the future cases which, compared to other rainfalls, is a more significant difference. Furthermore, with the applied evapotranspiration of 0.97mm, the effective discharge for the reference period is -0.87mm while the effective discharge for the future cases is 1.40mm, 1.56mm, and 2.11mm respectively. Similar cases can be observed the 9th, 11th, 19th, and 27th where the effective discharge is negative for the reference case and significantly higher for the future cases.

A similarity in shape of the lines among all the investigated cases can be observed both where the safety factor increases and decreases. This is particularly evident between the 19th and 21st for the reference case and between the 17th and 20th for the future cases where essentially the same inclination is obtained, see Figure 5.11. Another clear example of this is the 29th where the recovery after the heavy rainfall is observed to be very similar. A slightly steeper inclination is observed for the recovery of low safety factors, indicating a faster recovery for more severe cases. The most rapid decrease in safety factor for a 24-hour-period is 0.23 and is found on the 30th for the reference case. Decreases, similar in magnitude are identified where a heavy rainfall occurs directly after a day with little to no precipitation. Similar to the fastest decrease, the fastest recovery of the safety factor is found to be around 0.23 on several days during the month. Typically, these are found after a significant rainfall or period of rain, followed by a day or period with little to no precipitation.

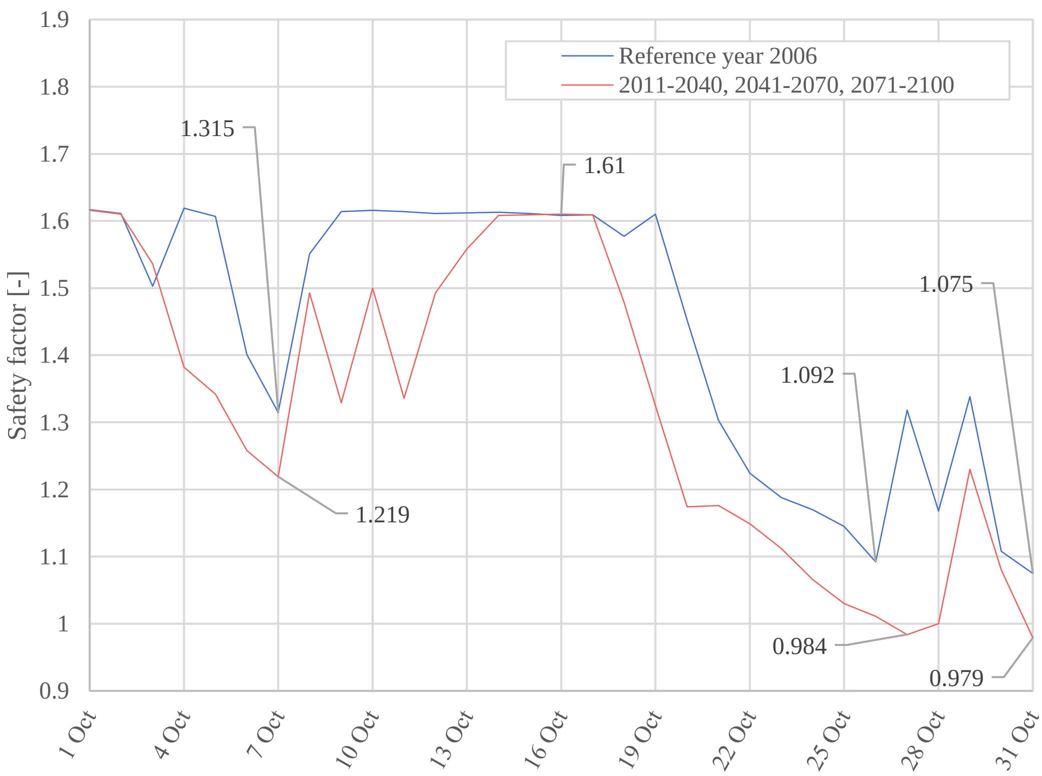

Figure 5.11. Safety factor for all cases in scenario 2.

The suction in point A and point B for scenario 2 is presented in Figure 5.12 and Figure 5.13. It is observed that the future cases are, like previous analyses, identical and the difference is rather between the reference year and the future scenarios. During the first days of October when several moderate rainfalls occurred, a steady decrease of suction is observed for point A, starting from the value of 12.58kPa. In point B during the same time, the suction is approaching 0kPa. At the 4th, a slight decrement is seen for the reference case in point A while a full recovery to 10.27kPa is observed for the reference case in point B. At this date, a precipitation of 0.1mm was introduced for the reference case which, similar to the effect on the safety factor, has no effect due to the evapotranspiration.

For point A, the shape of the curve can be seen to exponentially decrease as well as exponentially increase during rainfalls and recession of rainfalls respectively. During longer times of no precipitation, most notably observed between the 7th and 17th for the reference case in point A, the suction is approaching an equilibrium. The value of the equilibrium resembles the predicted, converging value for scenario 1. The equilibrium in point B is reached after a shorter time as it stagnates at around 10.2kPa after a single day of low precipitation. Like the safety factors, the rate of decrease and increase of the suction during similar conditions are more or less equal between the reference case and the future prognoses. Only a slightly faster recovery can be observed at times when the suction is lower, for example observed in Figure 5.12 between the 7th and 8th of October. During the month, the suction for the future cases is lower than for the reference year except when the two are equal.

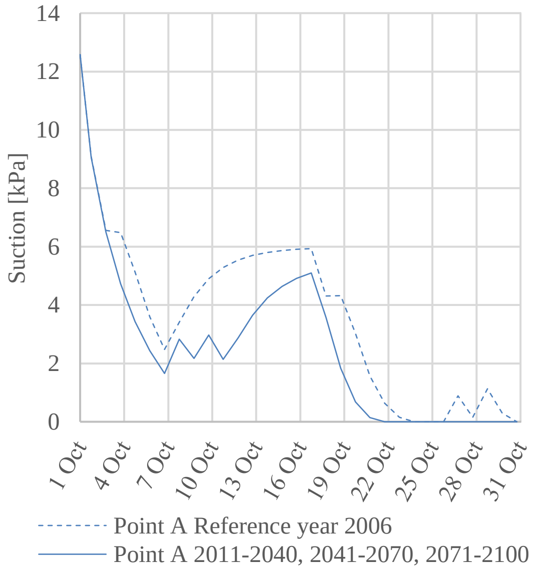

Figure 5.12. Suction in point A for the reference year and future cases in scenario 2.

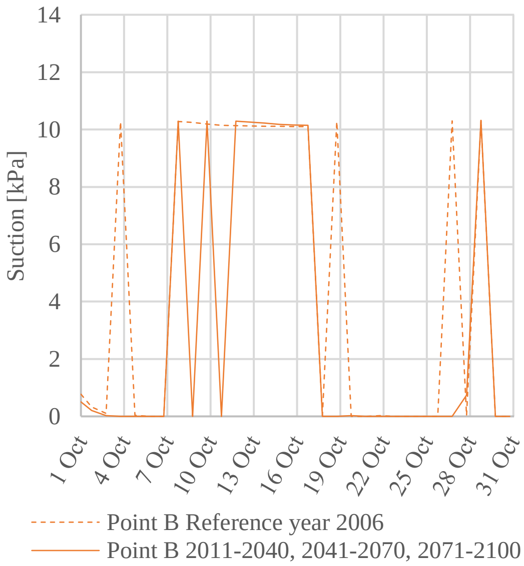

Figure 5.13. Suction in point B for the reference year and future cases in scenario 2.

5.2.3 Failure mechanisms

Figure 5.14 and Figure 5.15 displays the general shape of the two types of slip surfaces obtained in the investigation. Figure 5.14 shows the slip surface after more than three days of consecutive precipitation. Figure 5.15, on the other hand, shows the slip surface while little to no precipitation is introduced in the calculations. While long duration rainfalls suggest a toe failure on the upper section of the slope, short duration rainfalls or no rainfall, suggest a base failure for the entire formation. Essentially, the slip surface indicates a rotational failure mechanism which would mean that the slope fails along the slip surface.

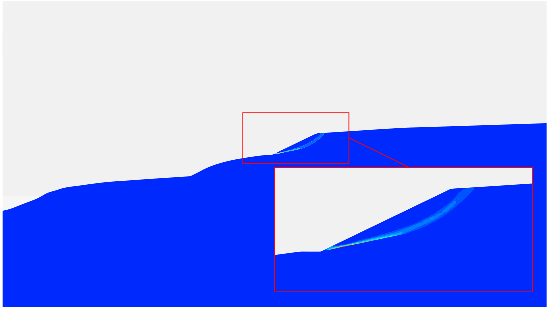

Figure 5.14. Slip surface after longer periods of precipitation.

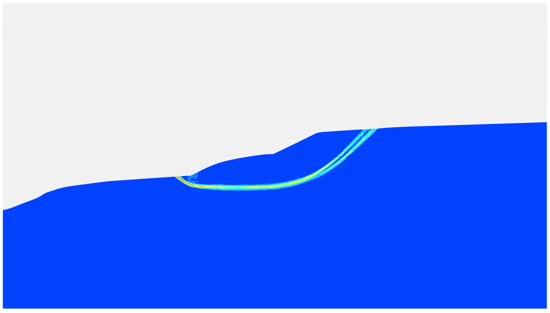

Figure 5.15. Slip surface after little to no precipitation.

6 Discussion

In the following chapter a discussion regarding the validity of the results from the precipitation predictions and the PLAXIS-simulations will be analysed. Additionally, uncertainties and assumptions related to the study will be presented.

6.1 The effects of future rainfalls on slope stability

From the extreme rainfall increase, it was noted that an identical increase applies for the first interval, 2011-2040, and the second interval, 2041-2070. This is due to the large uncertainty for short-term prognoses. Even though the predicted increase for the second interval were larger than the first, a similar increase was obtained due the large standard deviation for short-term prognoses.

A consideration of additional natural variations such as wind, sea level rise and potential earthquakes would possibly influence the result. As mentioned in 2.1.3.1, the wind pattern and intensity affect the evapotranspiration thus assigning a constant value would presumably not reflect reality. Also, climate change will inevitably affect the evapotranspiration as well which would imply that further investigation regarding the phenomena should be conducted. Furthermore, the evapotranspiration rate varies between both days and time of the day and the most accurate representation would be to assign a varying value. As the results suggested, the evaporation held a great influence on the small rainfalls by eliminating rainfall volumes. This would mean that days with no rain were simulated even though minor rainfalls occurred. From the result it was also observed that the safety factor during the lowest precipitation events were affected the most due to the evapotranspiration constituting a larger part than the rainfall itself. This would mean that the evaporation exceeded the rain volume, ultimately turning the effective discharge for certain rainfalls to negative. However, with the future increase added, a positive value was obtained for certain rainfalls which entailed a reduction of the safety factor, thus the difference between the two. In reality, the evaporation rate would not dissipate small rainfalls, rather the process of infiltration and evaporation would operate simultaneously. Ultimately, this means that even the lowest precipitation event would affect the safety factor of the slope to some extent and the evaporation would slowly dissipate the effect rather than remove it entirely as defined in the study. This does, however, only apply to short timeframes and during an entire day, the effective discharge could still be negative.

The hydrological property of the dry crust is another aspect that greatly influenced the results following small precipitation volumes. Since the permeability was assumed to be 1.4mm/day, a rainfall larger than this would exceed the infiltration capability and act as surface run-off. A higher permeability, which is often found in more coarse-grained materials, would imply that full saturation is reached more rapidly since the soil has more infiltration capability. Ultimately, this would mean that less surface run-off can be expected. For future, more voluminous rainfalls, such a scenario would entail that the minimum safety factor is obtained quicker than for the reference years, provided that the reference rainfall does not exceed the infiltration capability. If a reference rainfall volume surpasses the permeability interval, a future rainfall would not have additional effect on the safety factor of the slope as seen in the results when the safety factors are equal. The scenario with a higher permeability means that more apparent differences would possibly have been observed between future rainfalls.

It was observed that consecutive days of rain are more critical for the stability of the slope rather than the most extreme. This is most probably due to the low infiltration capability and therefore that full saturation requires a more prolonged period of precipitation. It was however, also observed that the suction seems to converge to an equilibrium during periods of no rain. The equilibrium for point B is reached after 1 day but for point A, an equilibrium is never fully reached as seen in Figure 5.12 and Figure 5.13. This would indicate that an extra period of no precipitation should have been added to both scenarios before day 1 to allow the suction to stabilise. Furthermore, a comparison between Figure 5.12 to Figure 5.13 and Figure 5.11 shows that the safety factor keeps decreasing during times of no suction in the slope. This would mean that not only the dissipation of the suction itself but the time which it is not present affects the safety factor.

6.2 Climate uncertainties

The presumably largest uncertainty in the result is the climate projections and how that relates to increased precipitation, both globally and locally. Even though almost every climate projection suggested an increase of both precipitation intensity and quantity for future scenarios, it is evidently difficult to say how it will unfold. Despite the broad knowledge of global warming, a precipitation prediction for an individual location is affected by more parameters than just temperature increase. With the respect to rainfall, there are additional factors that are crucial to predict the possible outcome. Some of these include wind patterns, ocean currents, plants, and soil compositions which might to come change with time [57]. As previously in history, there have occurred unpredictable events that have caused the climate to take rapid turns and therefore extensive climate projections to be re-written. Generators of such could be both natural and humanitarian that abruptly can change the climate and the conditions on the planet [58]. In terms of greenhouse gases emitted from human activity, three societal factors do primarily determine which path the emission scenario takes. These are global population, technology, and politics. There is no doubt that the global population is rising and, unless unpredictable events such as global diseases, war, or natural disasters occur, the population will continue to grow. A larger population does not necessarily mean higher emissions; however, it would put more pressure on sustainable climate strategies.

The climate models ECHAM-4 and -5 utilized by the Swedish Commission on Climate and Vulnerability has since the publication been superseded by the updated ECHAM-6 [59]. However, an adaption for the Swedish conditions have yet to be performed with the new climate models, thus the previous evaluation was utilized. The new model improved upon several factors, including temperature and precipitation, however slightly. The older models evidently have a minor exaggeration of long-term temperature and precipitation increase which ultimately means that the worst-case scenarios defined in this study are slightly overestimated. The differences are arguably marginal for Sweden at fractions of degrees and millimetres of rain. The largest differences between the models are found at the geographic poles and in the oceans of the planet. The difference this would impose on the acquired results are deemed negligibly small in this specific case but the importance of continued evolution of the climate models is acknowledged.

6.3 Estimation of parameters

The estimations and assumptions made for this study were carefully chosen in accordance with conventional parameter derivation methods and were deemed reasonable. The estimation of the stiffness modulus E’, and Possion ratio υ’ were defined according to typical values and since the parameters do not affect the flow calculations, they were deemed adequately accurate for the study. For the SWCC, the curve utilized in the study was not location-specific for the investigated slope, hence the soil-suction behavior can, and most likely will, differ from the reality. In order to find the actual SWCC for the soil composition in Hjärtum, either laboratory tests or an estimation with mathematical formulas would have to have been performed. This would arguably reflect reality more accurately, though the required data was, for this study, unavailable. Ideally it would have been most accurate to retrieve and derive data that are specific for the studied location. However, due to certain limitations, desired data is not always available which requires assumptions and estimations to be made.

6.4 Method analysis

The method was designed in order to obtain the results required to answer the research questions. However, a handful of boundaries and uncertainties limited the investigation to a certain degree. The approach of using Mohr-Coulomb as defining material model should be taken into consideration when evaluating the results. Since the model is relatively simple and aims to get a first estimation of a simulation, another calculation model could give contrasting results.

The collected weather data was limited to Gothenburg which in fact is a relatively long distance from Hjärtum, Lilla Edet. Despite this, the assumption that the climate in Hjärtum is close to identical to Gothenburg's was deemed representative for the study. However, it should be considered that Gothenburg is a coastal city and while Lilla Edet is located further north and inland, a slightly different precipitation pattern can be expected. Historically, the two sites have experienced very similar precipitation patterns over longer periods of time with the analysed year in 2006 only differing 2.8% in total precipitation. However, specifically for the examined months, a more noticeable difference is identified. In terms of total precipitation for October 2006, the closest located weather station to Lilla Edet recorded 43.9% less than Göteborg A. The historically rainiest months of the location does however slightly exceed the rainiest months in Gothenburg in terms of total precipitation. The similarity regarding long-term total precipitation therefore justifies the validity of scenario 2.

During the extreme rainfall in 1997, the precipitation recorded in Lilla Edet was 53.0mm compared to 85.7mm in Gothenburg, i.e., 33.7% lower. However, the most extreme rainfall event to be recorded in Lilla Edet during the reference period was slightly higher than the one on august 28th 1997 at 68.3mm which is roughly 20% less than the most extreme rainfall event in Gothenburg. This is arguably, still a relatively large difference and the validity of extreme rainfall predictions is lower than that of the monthly precipitation prediction. However, since hourly and more extensive data-series were unavailable for the closest located weather stations to Lilla Edet, a more precise evaluation of extreme rainfalls could not have been conducted with the available data.

The approach of using the worst-case scenarios from the climate models means that the most extreme and rare cases are examined. Since the extreme cases are based on the upper boundary of each interval, it would induce even more uncertainties for the estimations. The worst-case projection together with the extreme reference years, means a low probability of a rainfall with such magnitude. Even though the simulated rainfalls are extreme cases, a possibility of such rainfalls exists and should not be ignored. The strategy of separating winter and summer as two different seasons for precipitation increase in scenario 2 could be rather abrupt. In reality, a more gradual transition between months would be more reasonable, meaning that a potential increase or decrease does not shift over night between summer and winter months.

For scenario 2, a correction for extreme rainfalls was conducted for all rainfalls exceeding 1 year of reoccurrence time. In the specific case of October 2006, only one rainfall had a reoccurrence time greater than 1 year and was thus the only one being corrected. It could be seen as contradictory to correct scenario 2 with the method from scenario 1 when no rainfalls in the first scenario was corrected with the method used in the second one. However, the two scenarios can still be seen as two extreme cases where scenario 1 shows the effects of prolonged period of no rain followed by the most extreme. Scenario 2, on the other hand, shows the effects of both prolonged precipitation together with a rather extreme single rainfall.

The assumption that Clausius Clapeyron's theory of increased precipitation due to raised temperature hold for all types of rainfalls, can be argued. In fact, the Clausius Clapeyron relationship is more complex than that and depend upon several factors such as location, relative humidity, and duration of a rainfall. Studies have shown that a scaling, i.e., a non-linear relationship, of the air-vapor relation more accurately predict the intensification of precipitation events [60]. For instance, daily extreme rainfalls have shown to follow the Clausius Clapeyron rate while hourly extreme rainfalls exceed the rate and is more sensitive to temperature, thus leading to an intensification of more than 7%. After all, the theory has its limitations and does not correlate fully with reality, however it was deemed adequately accurate for a future prediction. Interestingly, if the Clausius Clapeyron theory was applied directly according to the temperature increase, an even higher total precipitation volume would have been obtained. Ultimately, this would suggest that the estimation done for this study underestimates the influence that the air-vapor relation has on precipitation.

Another uncertainty with the method was the strategy of adding precipitation increase to the days when a rainfall already occurred. It would be impossible to predict precise weather conditions for a future year, hence a simplification was made. The purpose was to examine the influence of total precipitation increase rather than finding particular days when rainfall occurs.

6.5 Recommendation for further studies

One assumption made was that the groundwater table was constant throughout the entire calculation and that it also did not change with season or for the future predictions. The defined groundwater table correlates to the highest water level in Göta älv and was deemed the worst-case scenario due to the potential of the suction being the lowest. A lower groundwater table should in theory allow for more suction and thus a higher safety factor. To which extent a higher or lower groundwater table affects the stability of a slope during rainfall scenarios could be examined in further studies.

Furthermore, another scenario excluded in the study was the effect that precipitation in the form of snow might have on the slope. If snow would be present for a longer period of time it could introduce a load which is more than negligible. The load could affect the safety factor both positively and negatively, depending on how it would be scattered. It would most probably be extended over the entire slope and work as much as a driving force as it would a resisting. The prediction is evidently that the winter season will experience the most increase in precipitation, however, this is mainly due to the larger increase in temperature which would imply less risk for snowy conditions. There is, nonetheless, the risk that an increased amount of snow could fall over the slope and act as a critical load for an extended period of time. The worst implication this could entail is not necessarily the load itself but rather the infiltration during melting. If the snow were to melt during a longer time in combination with additional precipitation, the suction for the slope might be 0 for an extended period as well. As seen in the result, the safety factor is at its lowest first after an extended period with low to no suction in the slope which could make this an implication. An evaluation of such scenarios is a valid idea for further studies as well.

The most significant rainfall events occur in the end of each month examined. In August of 1997 it was the 26th on which the largest rainfall occurred and in October of 2006, the largest rainfall took place on the 28th which was also surrounded by many other heavy rainfalls. Since the analysis begun at the start of the month, the majority of the calculation takes place before the most interesting results. This is more the case for scenario 1 than scenario 2 which is rather examining the effect of more prolonged and intense precipitation conditions. Since close to no precipitation events occurred early in August 1997, it would possibly have been better to examine a 30-day period rather than a specified month where the period would begin when the rainfall did. Furthermore, if a higher permeability was to be used, the results would have been more interesting if a single day was examined. If studies similar to this ever is performed, it is recommended to take these aspects into consideration.

7 Conclusion

The aim of the study was to examine the effects that historical and future severe rainfalls have on the stability of natural slopes. The report was also intended to act as a foundation for further studies regarding the effect that precipitation has on slope stability. This aim has been fulfilled by answering the three research questions introduced in the beginning of the study.

- *How will precipitation conditions in Västra Götaland evolve until the year 2100?*

The uncertainty and difficulty of predicting future precipitation conditions, and climate change in general, is palpable. This is particularly noticeable in the climate models and national precipitation evaluations that this study is based upon. This study separates total precipitation increase and the influence that climate change has on extreme rainfall events. In Västra Götaland, the precipitation prognoses suggest an increase and/or a decrease of total precipitation for the summer months. For winter months, on the other hand, an increase is solely predicted. The frequency of extreme rainfalls will increase and rainfalls with present intensity could be re-defined with future scaling. A conclusion from the precipitation prediction is that both more and heavier rainfalls can be expected in the future, with the year 2100 being the most severe.

- *To what extent will the safety factor of natural slopes be affected by the most extreme rainfall scenarios in the future compared to the most extreme rainfall scenarios today?*

As the result suggested, a future increase does not necessarily affect the stability of the investigated slope. The most notable difference was observed for minor rainfalls and days with no rain, where the added increase exceeded the evapotranspiration. It was also found that the permeability of the soil layers is crucial for the infiltration capacity and thus the suction of a slope. A higher permeability would entail a higher infiltration capability hence enabling fully saturated conditions to be reached more rapidly. Ultimately, this would mean that future rainfalls would have reduced the safety factor additionally, provided that the reference rainfall, as well as the increased rainfall, lies within the permeability interval. Such a scenario would possibly entail more apparent differences for future rainfalls.

- *Is the month with the single most extreme rainfall event or the month with the most total precipitation more critical for the stability of a slope?*

It was found that the month with *the most* precipitation was more critical for the stability of the slope, rather than the month with the most extreme *single* rainfall. While the rainiest month yielded a safety factor below 1, the single extreme rainfall scenario indicated a safety factor of 1.252.

It can thereby be concluded that in cases with a permeability lower than the precipitation rate, more prolonged rainfalls have more impact than short duration rainfalls with high intensity. Therefore, the most critical future rainfall scenario for slope stability is, in the end, one where periods of rain unfold during a longer time, thus constantly eliminating the influence of suction.

References

[1] NASA, “Climate Change: How Do We Know?,” Feb. 08, 2022. https://climate.nasa.gov/evidence/ (accessed Feb. 11, 2022).

[2] Jeremy Wilks, “What was the role of climate change in Germany’s fatal floods?,” *EuroNews*, Oct. 18, 2021. https://www.euronews.com/green/2021/10/18/what-was-the-role-of-climate-change-in-germany-s-fatal-floods (accessed Feb. 11, 2022).

[3] SMHI, “2021 - Skyfall i Gävle,” Sep. 20, 2021. https://www.smhi.se/kunskapsbanken/hydrologi/historiska-oversvamningar/2021-skyfall-i-gavle-1.175548 (accessed Feb. 15, 2022).

[4] Swedish Commission on Climate and Vulnerability, “Sweden facing climate change,” Stockholm, 2007.

[5] T. V. Tran, M. T. Trinh, G. Lee, S. Oh, and T. H. van Nguyen, “Effect of Extreme Rainfall on Cut Slope Stability: Case Study in Yen Bai City, Viet Nam,” *Journal of the Korean Geoenvironmental Society*, vol. 16, no. 4, pp. 23–32, Apr. 2015, doi: 10.14481/jkges.2015.16.4.23.

[6] S. A. Anderson and N. Sitar, “Analysis of Rainfall-Induced Debris Flows,” *Journal of Geotechnical Engineering*, vol. 121, no. 7, 1995, doi: 10.1061/(ASCE)0733-9410(1995)121:7(544).

[7] H. Chen, C. F. Lee, and K. T. Law, “Causative Mechanisms of Rainfall-Induced Fill Slope Failures,” *Journal of Geotechnical and Geoenvironmental Engineering*, vol. 130, no. 6, 2004, doi: 10.1061/(ASCE)1090-0241(2004)130:6(593).

[8] D. G. Fredlund, “The Stability of Slopes with Negative Pore-water Pressures,” 1995. [Online]. Available: https://www.researchgate.net/publication/348279438

[9] United Nations, “What Is Climate Change?” n.d. https://www.un.org/en/climatechange/what-is-climate-change (accessed Feb. 11, 2022).

[10] National Academy of Sciences, *Climate Change: Evidence and Causes: Update 2020*. Washington, DC: The National Academies Press, 2020. doi: 10.17226/25733.

[11] NASA, “Is the Sun causing global warming?,” n.d. https://climate.nasa.gov/faq/14/is-the-sun-causing-global-warming/ (accessed Feb. 17, 2022).

[12] M. Denchak and J. Turrentine, “Global Climate Change: What You Need to Know,” Sep. 01, 2021. https://www.nrdc.org/stories/global-climate-change-what-you-need-know (accessed Feb. 11, 2022).

[13] NASA, “Climate Change: How Do We Know?,” Feb. 08, 2022. https://climate.nasa.gov/evidence/ (accessed Feb. 11, 2022).

[14] M. Denchak, “Greenhouse Effect 101,” Jul. 16, 2019. https://www.nrdc.org/stories/greenhouse-effect-101 (accessed Feb. 11, 2022).

[15] F. & R. A. Department for Environment and Environment Agency, “Calculate the carbon dioxide equivalent quantity of an F gas,” 2014. https://www.gov.uk/guidance/calculate-the-carbon-dioxide-equivalent-quantity-of-an-f-gas (accessed Mar. 24, 2022).

[16] United States Environmental Protection Agency, “Overview of Greenhouse Gases.” n.d. https://www.epa.gov/ghgemissions/overview-greenhouse-gases (accessed Mar. 24, 2022).

[17] European Commision, “Paris Agreement.” n.d. https://ec.europa.eu/clima/eu-action/international-action-climate-change/climate-negotiations/paris-agreement_en (accessed Feb. 11, 2022).

[18] V. Masson-Delmotte *et al.*, *Climate Change 2021*. Cambridge University Press, 2021. Accessed: Mar. 31, 2022. [Online]. Available: https://www.ipcc.ch/report/ar6/wg1/downloads/report/IPCC_AR6_WGI_SPM_final.pdf

[19] European Environmental Agnecy, “Sulphur dioxide (SO2) emissions,” 2014. https://www.eea.europa.eu/data-and-maps/indicators/eea-32-sulphur-dioxide-so2-emissions-1/assessment-3 (accessed Mar. 07, 2022).

[20] R. Lindsey and L. Dahlman, “Climate Change: Global Temperature,” 2021. https://www.climate.gov/news-features/understanding-climate/climate-change-global-temperature (accessed Feb. 17, 2022).

[21] United States Environmental Protection Agency, “Climate Change Indicators: Weather and Climate.” n.d. https://www.epa.gov/climate-indicators/weather-climate (accessed Feb. 17, 2022).

[22] European Commision, “Climate change consequences.” n.d. https://ec.europa.eu/clima/climate-change/climate-change-consequences_en (accessed Feb. 11, 2022).

[23] SMHI, “2021 - Skyfall i Gävle,” Sep. 20, 2021. https://www.smhi.se/kunskapsbanken/hydrologi/historiska-oversvamningar/2021-skyfall-i-gavle-1.175548 (accessed Feb. 15, 2022).

[24] F. Kreienkamp *et al.*, “Rapid attribution of heavy rainfall events leading to the severe flooding in Western Europe during July 2021,” n.d. Deutscher Wetterdienst. Accessed: Feb. 14, 2022. [Online]. Available: https://www.worldweatherattribution.org/wp-content/uploads/Scientific-report-Western-Europe-floods-2021-attribution.pdf

[25] Svenskt Vatten, “Rekommendationer vid val av nederbördsstatistik för dimensionering av dagvattensystem,” Apr. 2020. Accessed: Feb. 11, 2022. [Online]. Available: https://www.svensktvatten.se/globalassets/rornat-och-klimat/klimat-och-dagvatten/svensktvatten_smhi_pm-april-2020.pdf

[26] M. Martinkova and J. Kysely, “Overview of observed clausius-clapeyron scaling of extreme precipitation in midlatitudes,” *Atmosphere*, vol. 11, no. 8. MDPI AG, Aug. 01, 2020. doi: 10.3390/ATMOS11080786.

[27] Water Science School, “The 100-Year Flood,” *United States Geological Survey*, Jun. 07, 2018. https://www.usgs.gov/special-topics/water-science-school/science/100-year-flood (accessed Feb. 16, 2022).

[28] B. Dahlström, “Regnintensitet,” Stockholm, 2010. Accessed: Feb. 14, 2022. [Online]. Available: https://vav.griffel.net/filer/Rapport_2010-05.pdf

[29] SMHI, “Avdunstning,” 2022. https://www.smhi.se/kunskapsbanken/hydrologi/vattnets-kretslopp/avdunstning-1.30720 (accessed Jun. 02, 2022).

[30] J. Olsson and K. Foster, “Extrem korttidsnederbörd i klimatprojektioner för Sverige,” 2013. Accessed: Feb. 21, 2022. [Online]. Available: https://www.smhi.se/polopoly_fs/1.164975!/Klimatologi_6%20Extrem%20korttidsnederb%C3%B6rd%20i%20klimatprojektioner%20f%C3%B6r%20Sverige.pdf

[31] RSA GEOTECHNICS LTD, “Slope stability analysis.” n.d. https://www.rsa-geotechnics.co.uk/geotechnical-engineering-2/slope-stability-analysis/ (accessed Feb. 17, 2022).

[32] GeoEngineer, “Slope Stability: Critical Failure Surface & Design Factor of Safety.” n.d. https://www.geoengineer.org/education/slope-stability/slope-stability-critical-failure-surface-design-factor-of-safety (accessed Feb. 17, 2022).

[33] Bentley, “PLAXIS 2D-Reference Manual,” Dec. 2021. Accessed: Feb. 17, 2022. [Online]. Available: https://communities.bentley.com/cfs-file/__key/communityserver-wikis-components-files/00-00-00-05-58/PLAXIS2D_2D00_CE_2D00_V22.00_2D00_2_2D00_Reference.pdf

[34] The Constructor, “Types of Slope Failures.” n.d. https://theconstructor.org/geotechnical/slope-failures-types/28467/ (accessed Jun. 02, 2022).

[35] V. Galavi, “Groundwater flow, fully coupled flow deformation and undrained analyses in PLAXIS 2D and 3D,” 2010.

[36] M. Li, H. Yu, and H. Du, “Prediction of capillary suction in porous media based on micro-CT technology and B–C model,” *Open Physics*, vol. 18, no. 1, pp. 906–915, Dec. 2020, doi: 10.1515/phys-2020-0203.

[37] H. Yokoi, “Relationship between soil cohesion and shear strength,” *Soil Science and Plant Nutrition*, vol. 14, no. 3, pp. 89–93, May 1968, doi: 10.1080/00380768.1968.10432750.

[38] Statens Geotekniska Institut, “Jords tekniska egenskaper,” 2019. https://www.sgi.se/sv/kunskapscentrum/om-geoteknik-och-miljogeoteknik/geoteknik-och-markmiljo/jordmateriallara/jords-tekniska-egenskaper/ (accessed Mar. 07, 2022).

[39] I.-H. Ho, S. Li, and L. Ma, “Analysis of Partially Saturated Clayey Slopes Using Finite Element Method,” *Soil Mechanics and Foundation Engineering*, vol. 56, no. 6, pp. 382–389, Jan. 2020, doi: 10.1007/s11204-020-09619-6.

[40] D. G. Fredlund, H. Rahardjo, and M. D. Fredlund, *Unsaturated Soil Mechanics in Engineering Practice*, 1st ed. John Wiley & Sons, Incorporated, 2012.

[41] P. Jayathilaka, B. Indraratna, and A. Heitor, “Influence of Salinity-Based Osmotic Suction on the Shear Strength of a Compacted Clay,” *International Journal of Geomechanics*, vol. 21, no. 5, p. 04021041, May 2021, doi: 10.1061/(ASCE)GM.1943-5622.0001988.

[42] B. GHANBARIAN-ALAVIJEH, A. LIAGHAT, G.-H. HUANG, and M. Th. van GENUCHTEN, “Estimation of the van Genuchten Soil Water Retention

Properties from Soil Textural Data," *Pedosphere*, vol. 20, no. 4, pp. 456–465, Aug. 2010, doi: 10.1016/S1002-0160(10)60035-5.

[43] M. Azmi, M. H. Ramli, M. A. Hezmi, S. A. N. Mohd Yusoff, and M. N. A. Alel, "Estimation of Soil Water Characteristic Curves (SWCC) of mining sand using soil suction modelling," in *IOP Conference Series: Materials Science and Engineering*, 2019, vol. 527, no. 1. doi: 10.1088/1757-899X/527/1/012016.

[44] A. Taban, M. . M. Sadeghi, and M. A. Rowshanzamir, "The Estimation of van Genuchten SWCC Model for Unsaturated Sands by means of the Genetic Programming," *Scientia Iranica*, vol. 0, no. 0, pp. 0–0, Aug. 2017, doi: 10.24200/sci.2017.4206.

[45] GEO-SLOPE International Ltd., "Seepage Modeling with SEEP/W," Alberta, 2012. Accessed: Mar. 18, 2022. [Online]. Available: https://downloads.geo-slope.com/geostudioresources/8/0/6/books/seep%20modeling.pdf?v=8.0.7.6129j

[46] S. Knutsson, R. Larsson, M. Tremblay, and A.-L. Öberg-Högsta, "Siltjordas egenskaper," Linköping, 1998. Accessed: Apr. 18, 2022. [Online]. Available: https://www.sgi.se/globalassets/publikationer/info/pdf/sgi-i16.pdf

[47] H. Yang, H. Rahardjo, E.-C. Leong, and D. G. Fredlund, "Factors affecting drying and wetting soil-water characteristic curves of sandy soils," *Canadian Geotechnical Journal*, vol. 41, no. 5, pp. 908–920, Sep. 2004, doi: 10.1139/t04-042.

[48] J. F. Labuz and A. Zang, "Mohr–Coulomb Failure Criterion," *Rock Mechanics and Rock Engineering*, vol. 45, no. 6, pp. 975–979, Nov. 2012, doi: 10.1007/s00603-012-0281-7.

[49] A. A. Tagar *et al.*, "Finite element simulation of soil failure patterns under soil bin and field testing conditions," *Soil and Tillage Research*, vol. 145, pp. 157–170, Jan. 2015, doi: 10.1016/j.still.2014.09.006.

[50] Arne Forsman, "Göta älv," n.d. *Nationalencyklopedin*. Accessed: Mar. 18, 2022. [Online]. Available: https://www.ne.se/uppslagsverk/encyklopedi/l%C3%A5ng/g%C3%B6ta-%C3%A4lv

[51] Göta älvs Vattenvårdförbund, Sweden. *Fakta om Göta älv*, (2015). Accessed: Mar. 28, 2022. [Online Video]. Available: https://www.gotaalvvvf.org/download/18.2f0ad835166c596881356a83/1540998119692/fakta_om_gota_alv_webb.pdf

[52] Swedish Geological Institute, "Skredrisker i Göta älvdalen i ett förändrat klimat," Linköping, 2012. Accessed: Apr. 18, 2022. [Online]. Available: https://www.sgi.se/globalassets/publikationer/gota-alvutredningen/gau_slutrapport_del2.pdf

[53] R. Larsson, "Jords egenskaper," Linköping, 2008. Accessed: Apr. 29, 2022. [Online]. Available: https://www.sgi.se/globalassets/publikationer/info/pdf/sgi-i1.pdf

[54] B. Eriksson, "Den Potentiella Evapotranspirationen i Sverige," 1981.

[55] F. Cheshmberah and A. A. Zolfaghari, "The Effect of Climate Change on Future Reference Evapotranspiration in Different Climatic Zones of Iran," *Pure*

and Applied Geophysics, vol. 176, no. 8, pp. 3649–3664, Aug. 2019, doi: 10.1007/s00024-019-02148-w.

[56] S. Kumar Thota, T. Duc Cao, and F. Vahedifard, “Poisson’s Ratio Characteristic Curve of Unsaturated Soils,” *Journal of Geotechnical and Geoenvironmental Engineering*, vol. 147, no. 1, p. 04020149, Jan. 2021, doi: 10.1061/(ASCE)GT.1943-5606.0002424.

[57] Australian Academy of Science, “What are the uncertainties and their implications?,” https://www.science.org.au/learning/general-audience/science-climate-change/8-what-are-uncertainties-and?msclkid=264b9ca4c6e911ec9e10b402ec4a7373 (accessed Apr. 29, 2022).

[58] M. Latif, “Uncertainty in climate change projections,” *Journal of Geochemical Exploration*, vol. 110, no. 1, pp. 1–7, Jul. 2011, doi: 10.1016/j.gexplo.2010.09.011.

[59] S. Gui, R. Yang, and J. Cao, “Simulation Improvements of ECHAM5-NEMO3.6 and ECHAM6- NEMO3.6 Coupled Models Compared to MPI-ESM and the Corresponding Physical Mechanisms,” *Geoscientific Model Development*, 2018, doi: 10.5194/gmd-2018-130.

[60] J.-L. Martel, F. P. Brissette, P. Lucas-Picher, M. Troin, and R. Arsenault, “Climate Change and Rainfall Intensity–Duration–Frequency Curves: Overview of Science and Guidelines for Adaptation,” *Journal of Hydrologic Engineering*, vol. 26, no. 10, p. 03121001, Oct. 2021, doi: 10.1061/(ASCE)HE.1943-5584.0002122.

Appendix A

Descriptive height map over Hjärtum, Lilla Edet, including boreholes and sections.

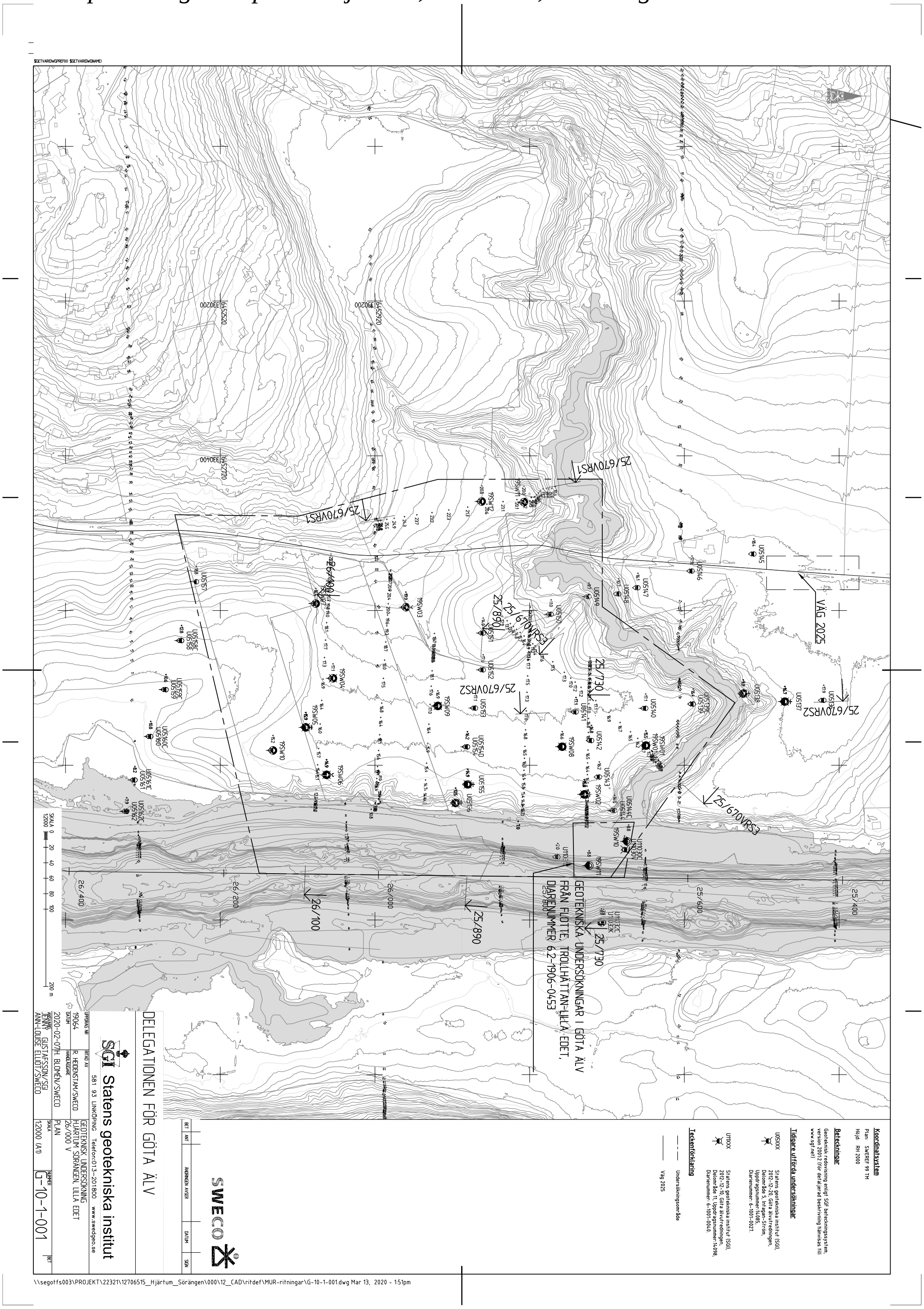

Appendix B

Precipitation projections for 10-year rainfalls in Sweden together with standard deviation.

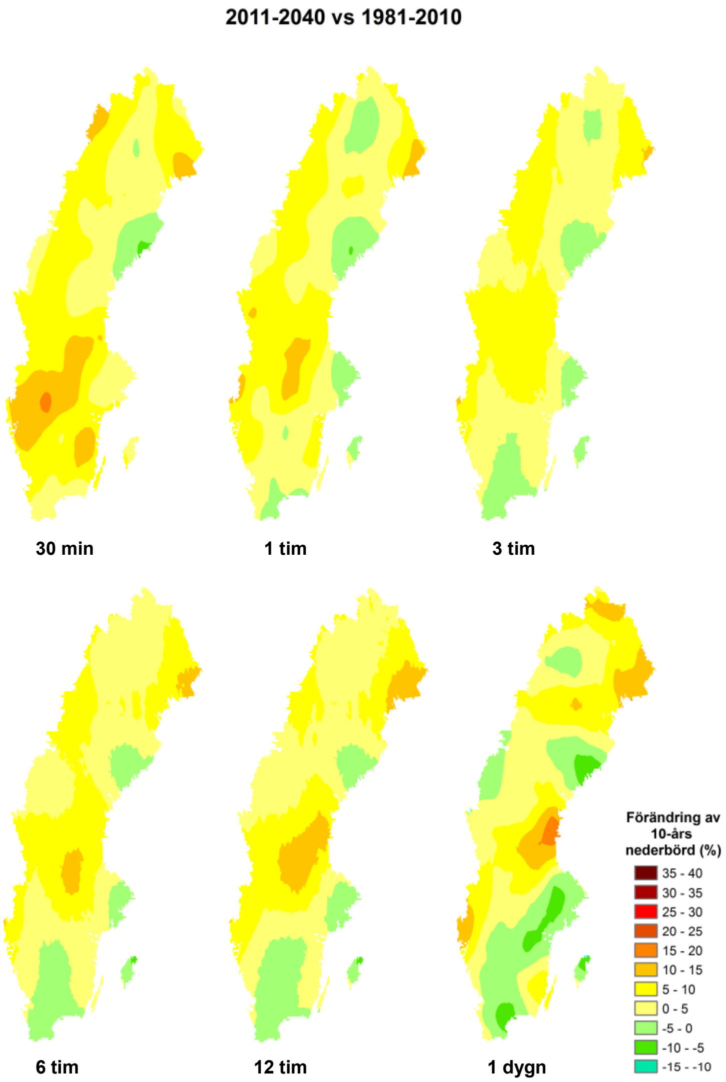

Figur 4. Medelvärdet av projektionernas förändring av korttidsnederbörd med 10 års återkomsttid från period R2 (1981-2010) till period F1 (2011-2040).

9

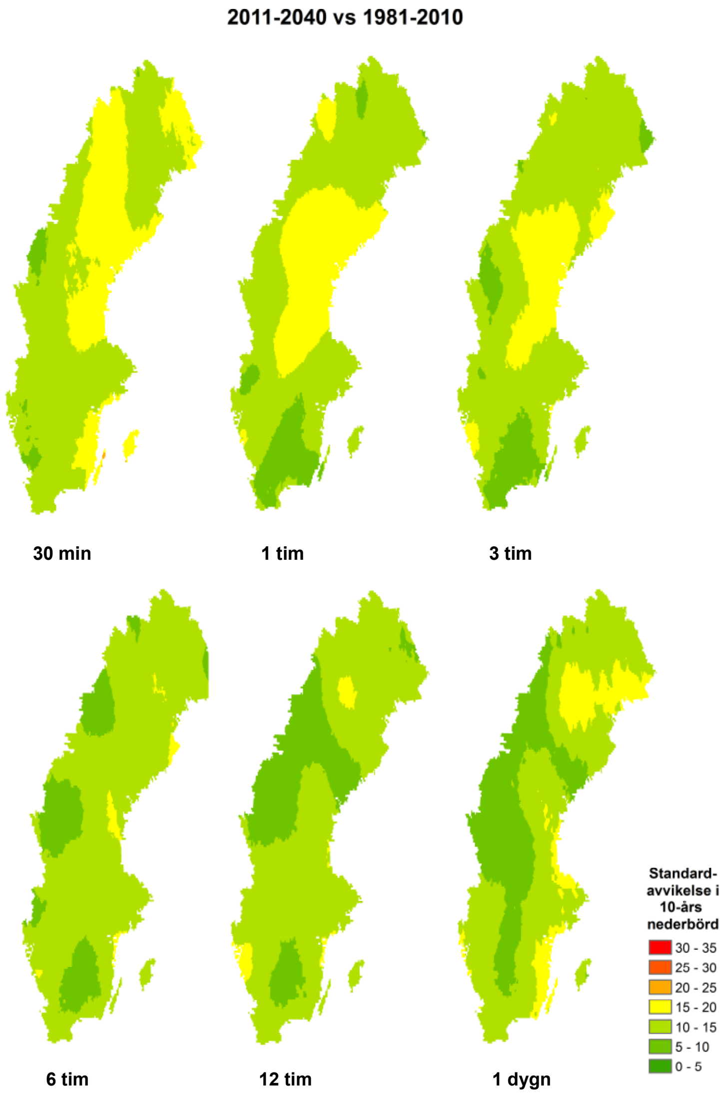

Figur 5. Standardavvikelsen för projektionernas förändring av korttidsnederbörd med 10 års återkomsttid från period R2 (1981-2010) till period F1 (2011-2040).

10

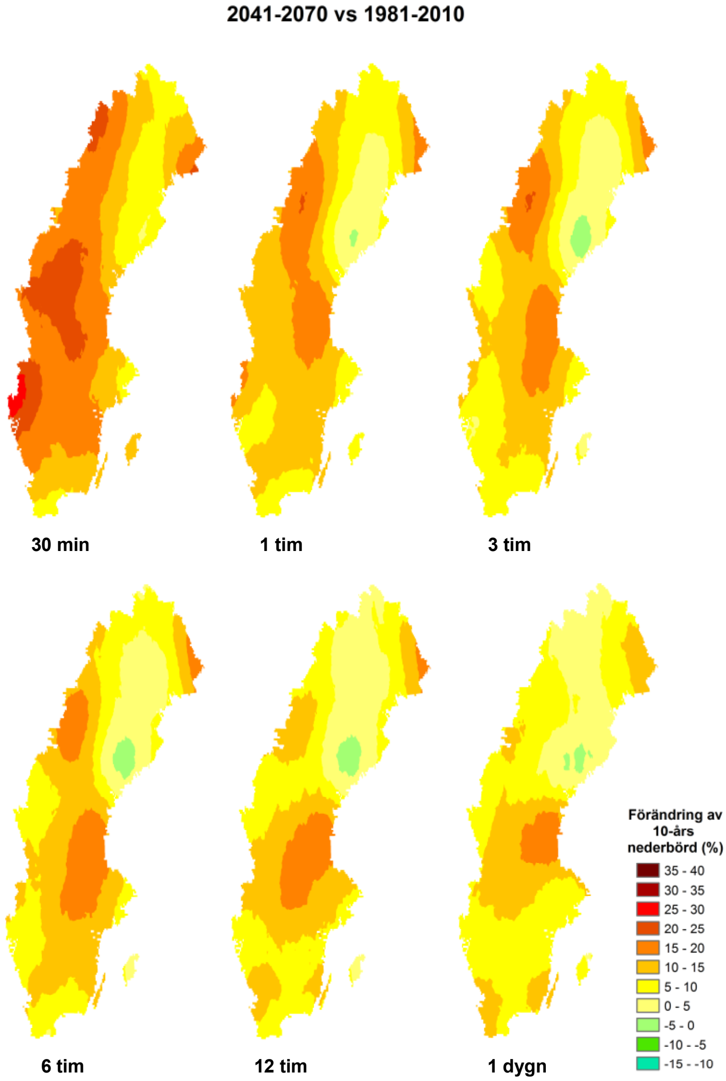

Figur 6. Medelvärdet av projektionernas förändring av korttidsnederbörd med 10 års återkomsttid från period R2 (1981-2010) till period F2 (2041-2070).

11

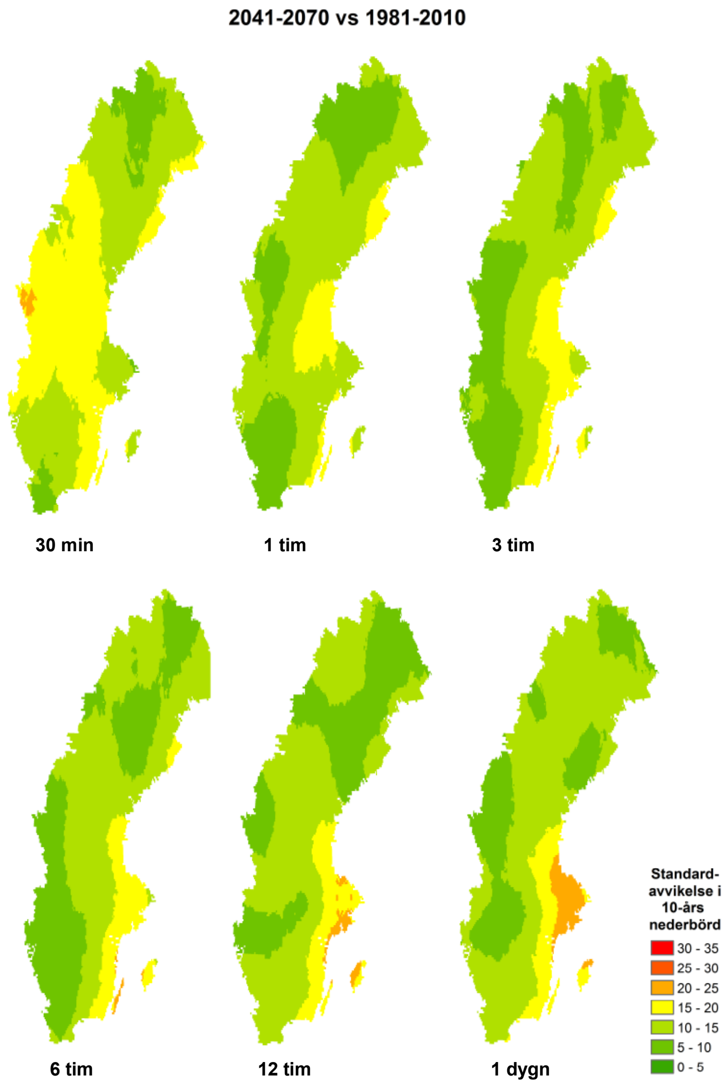

Figur 7. Standardavvikelsen för projektionernas förändring av korttidsnederbörd med 10 års återkomsttid från period R2 (1981-2010) till period F2 (2041-2070).

12

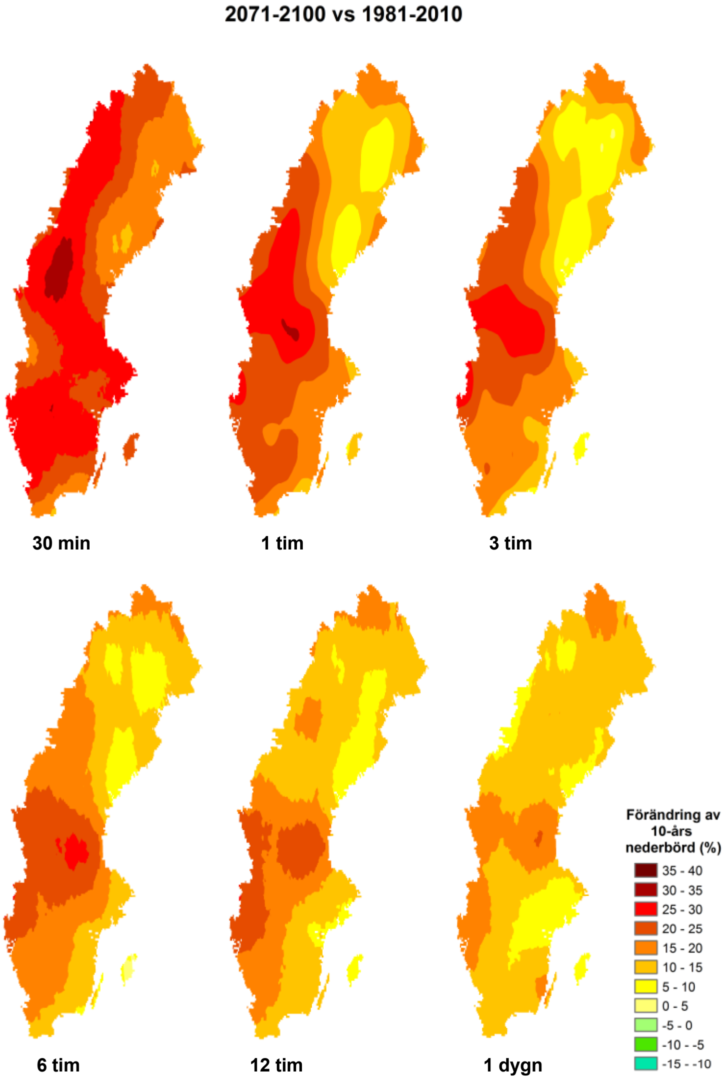

Figur 8. Medelvärdet av projektionernas förändring av korttidsnederbörd med 10 års återkomsttid från period R2 (1981-2010) till period F3 (2071-2100).

13

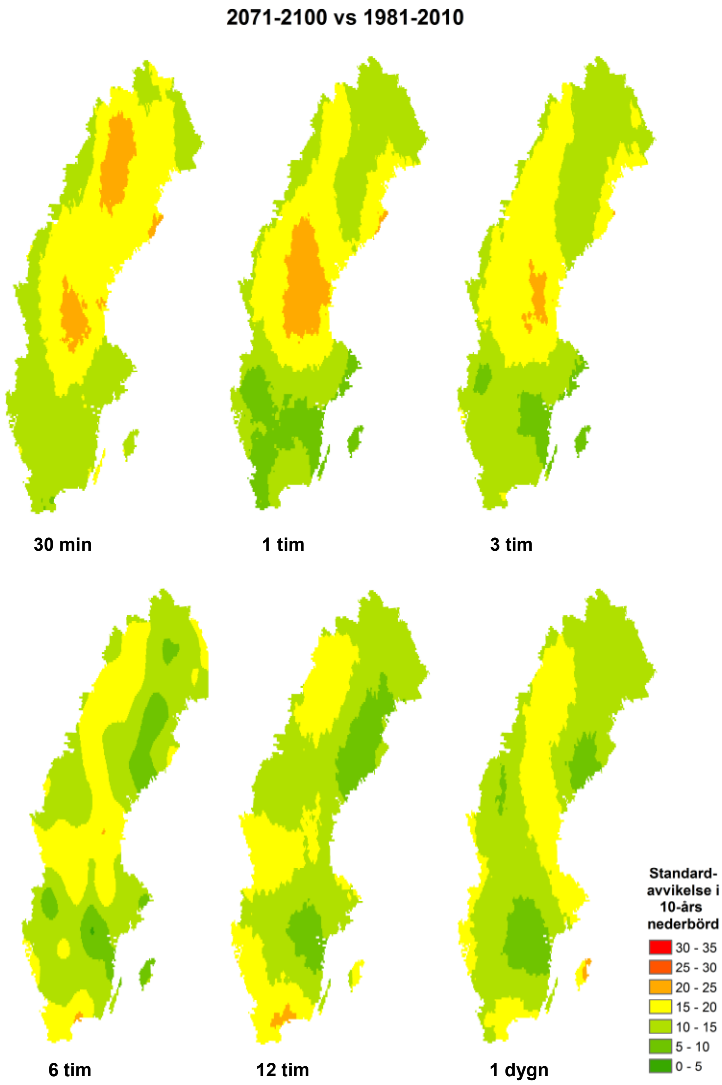

Figur 9. Standardavvikelsen för projektionernas förändring av korttidsnederbörd med 10 års återkomsttid från period R2 (1981-2010) till period F3 (2071-2100).

14

Appendix C

Derivation of values and parameters utilized in the study

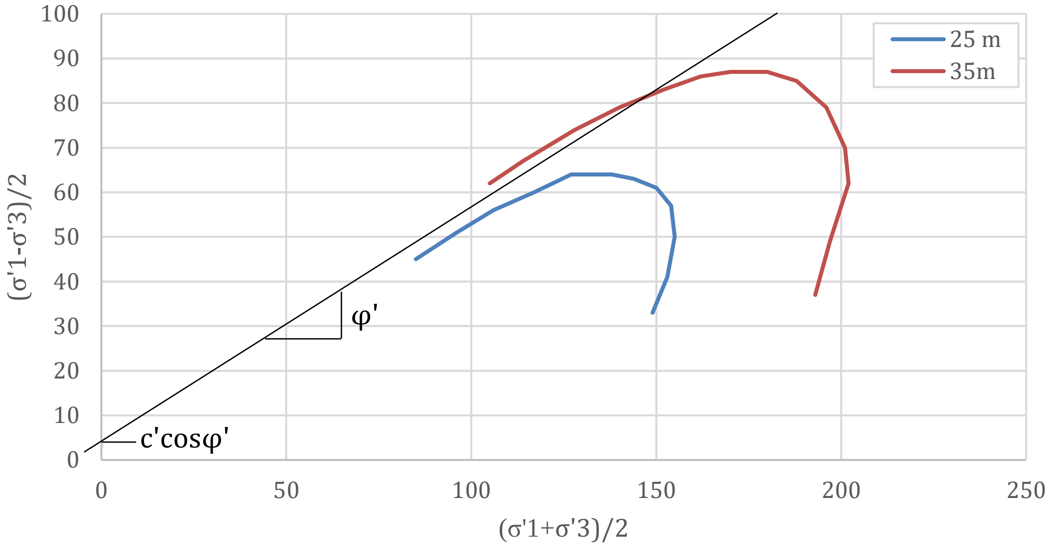

Figure C.1. Triaxial tests accompanied by a trendline intersecting the y-axis.

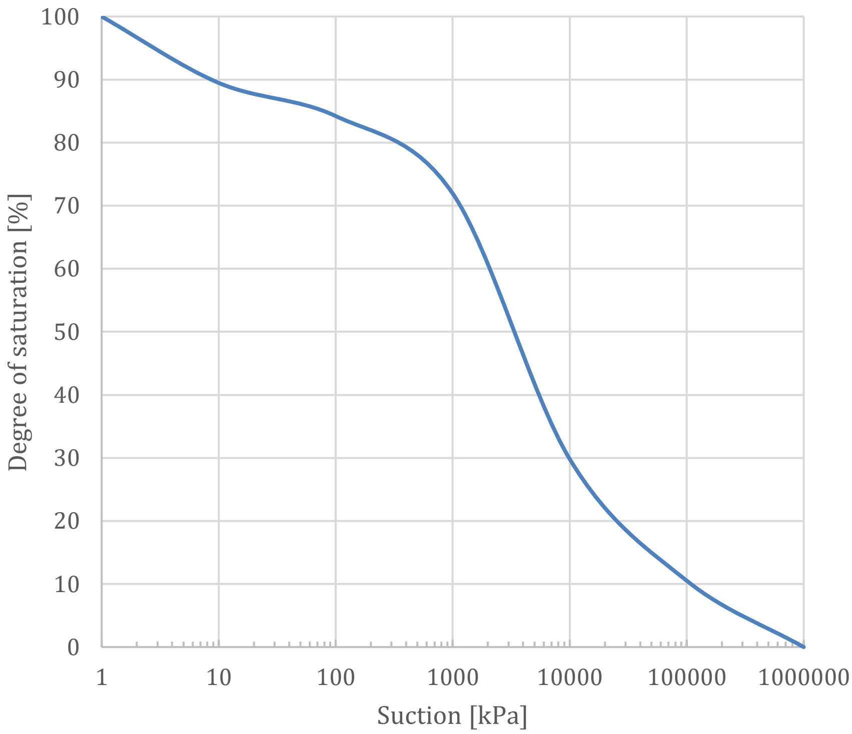

Figure C.2. Soil water characteristic curve.

Table C.1. Derived input parameters.

	Dry crust	Clay 1-3
Effective cohesion, c’	0.5	4.27
Stiffness modulus, E’	10E3	10E3
Poisson’s ratio	0.2	0.2
Friction angle	30°	30°
SWCC		
α	0.01186	0.01186
n	1.467	1.467
θ_r	0	0
θ_s	1	1

Appendix D

Tabulated values

Table D.1. Precipitation and effective discharge for the reference year 1997 as well as the future cases for scenario 1.

	Precipitation [mm]	Effective discharge [mm]			
	1997	1997	2011-2040	2041-2070	2071-2100
01-Aug	0	-3.226	-3.226	-3.226	-3.226
02-Aug	0	-3.226	-3.226	-3.226	-3.226
03-Aug	0	-3.226	-3.226	-3.226	-3.226
04-Aug	6.9	3.674	3.674	3.674	3.674
05-Aug	0	-3.226	-3.226	-3.226	-3.226
06-Aug	0	-3.226	-3.226	-3.226	-3.226
07-Aug	0	-3.226	-3.226	-3.226	-3.226
08-Aug	0	-3.226	-3.226	-3.226	-3.226
09-Aug	0	-3.226	-3.226	-3.226	-3.226
10-Aug	0	-3.226	-3.226	-3.226	-3.226
11-Aug	0	-3.226	-3.226	-3.226	-3.226
12-Aug	0	-3.226	-3.226	-3.226	-3.226
13-Aug	0	-3.226	-3.226	-3.226	-3.226
14-Aug	0	-3.226	-3.226	-3.226	-3.226
15-Aug	0	-3.226	-3.226	-3.226	-3.226
16-Aug	0	-3.226	-3.226	-3.226	-3.226
17-Aug	0	-3.226	-3.226	-3.226	-3.226
18-Aug	0	-3.226	-3.226	-3.226	-3.226
19-Aug	0	-3.226	-3.226	-3.226	-3.226
20-Aug	3.8	0.574	0.574	0.574	0.574
21-Aug	0	-3.226	-3.226	-3.226	-3.226
22-Aug	4.9	1.674	1.674	1.674	1.674
23-Aug	0.1	-3.126	-3.126	-3.126	-3.126
24-Aug	19.8	16.574	16.574	16.574	16.574
25-Aug	33.6	30.374	30.374	30.374	30.374
26-Aug	85.7	82.474	101.757	101.757	113.649
27-Aug	0.4	-2.826	-2.826	-2.826	-2.826
28-Aug	0	-3.226	-3.226	-3.226	-3.226
29-Aug	0	-3.226	-3.226	-3.226	-3.226
30-Aug	1.6	-1.626	-1.626	-1.626	-1.626
31-Aug	0	-3.226	-3.226	-3.226	-3.226

Table D.2. Safety factor for the entire slope and suction for point A and B for the reference year 1997 and the future cases in scenario 1.

	Safety factor [-]		Suction [kPa]			
	1997	2011-2100	1997 point A	2011-2100 point B	1997 point A	2011-2100 point B
01-Aug	1.639	1.639	14.408	14.408	22.690	22.690
02-Aug	1.636	1.636	14.109	14.109	15.320	15.320
03-Aug	1.633	1.633	12.729	12.729	13.070	13.070
04-Aug	1.611	1.611	9.799	9.799	9.531	9.531
05-Aug	1.628	1.628	8.796	8.796	10.160	10.160
06-Aug	1.618	1.618	8.429	8.429	10.100	10.100
07-Aug	1.619	1.619	8.240	8.240	10.160	10.160
08-Aug	1.617	1.617	8.060	8.060	10.160	10.160
09-Aug	1.617	1.617	7.884	7.884	10.150	10.150
10-Aug	1.617	1.617	7.718	7.718	10.130	10.130
11-Aug	1.616	1.616	7.564	7.564	10.110	10.110
12-Aug	1.615	1.615	7.423	7.423	10.090	10.090
13-Aug	1.616	1.616	7.295	7.295	10.080	10.080
14-Aug	1.615	1.615	7.178	7.178	10.060	10.060
15-Aug	1.614	1.614	7.072	7.072	10.050	10.050
16-Aug	1.615	1.615	6.975	6.975	10.050	10.050
17-Aug	1.616	1.616	6.886	6.886	10.060	10.060
18-Aug	1.615	1.615	6.805	6.805	10.060	10.060
19-Aug	1.618	1.618	6.730	6.730	10.060	10.060
20-Aug	1.602	1.602	5.104	5.104	0.067	0.067
21-Aug	1.612	1.612	5.103	5.103	10.280	10.280
22-Aug	1.539	1.539	3.755	3.755	0.000	0.000
23-Aug	1.613	1.613	4.059	4.059	10.280	10.280
24-Aug	1.462	1.462	2.932	2.932	0.000	0.000
25-Aug	1.339	1.339	1.589	1.589	0.000	0.000
26-Aug	1.252	1.252	0.680	0.680	0.000	0.000
27-Aug	1.448	1.448	1.887	1.887	10.300	10.300
28-Aug	1.528	1.528	2.918	2.918	10.260	10.260
29-Aug	1.603	1.603	3.636	3.636	10.250	10.250
30-Aug	1.607	1.607	4.112	4.112	10.220	10.220
31-Aug	1.610	1.610	4.438	4.438	10.190	10.190

Table D.3. Precipitation and effective discharge for the reference year 2006 as well as the future cases for scenario 2.

	Precipitation [mm]				Effective discharge [mm]			
	2006	**2011-2040**	**2041-2070**	**2071-2100**	**2006**	**2011-2040**	**2041-2070**	**2071-2100**
01-Oct	6.60	8.87	9.03	9.58	5.63	7.90	8.06	8.61
02-Oct	7.70	9.97	10.13	10.68	6.73	9.00	9.16	9.71
03-Oct	2.20	4.47	4.63	5.18	1.23	3.50	3.66	4.21
04-Oct	0.10	2.37	2.53	3.08	-0.87	1.40	1.56	2.11
05-Oct	3.80	6.07	6.23	6.78	2.83	5.10	5.26	5.81
06-Oct	18.20	20.47	20.63	21.18	17.23	19.50	19.66	20.21
07-Oct	8.10	10.37	10.53	11.08	7.13	9.40	9.56	10.11
08-Oct	0.00	0.00	0.00	0.00	-0.97	-0.97	-0.97	-0.97
09-Oct	0.70	2.97	3.13	3.68	-0.27	2.00	2.16	2.71
10-Oct	0.00	0.00	0.00	0.00	-0.97	-0.97	-0.97	-0.97
11-Oct	0.10	2.37	2.53	3.08	-0.87	1.40	1.56	2.11
12-Oct	0.00	0.00	0.00	0.00	-0.97	-0.97	-0.97	-0.97
13-Oct	0.00	0.00	0.00	0.00	-0.97	-0.97	-0.97	-0.97
14-Oct	0.00	0.00	0.00	0.00	-0.97	-0.97	-0.97	-0.97
15-Oct	0.00	0.00	0.00	0.00	-0.97	-0.97	-0.97	-0.97
16-Oct	0.00	0.00	0.00	0.00	-0.97	-0.97	-0.97	-0.97
17-Oct	0.00	0.00	0.00	0.00	-0.97	-0.97	-0.97	-0.97
18-Oct	5.70	7.97	8.13	8.68	4.73	7.00	7.16	7.71
19-Oct	0.10	2.37	2.53	3.08	-0.87	1.40	1.56	2.11
20-Oct	6.60	8.87	9.03	9.58	5.63	7.90	8.06	8.61
21-Oct	6.10	8.37	8.53	9.08	5.13	7.40	7.56	8.11
22-Oct	17.20	19.47	19.63	20.18	16.23	18.50	18.66	19.21
23-Oct	12.60	14.87	15.03	15.58	11.63	13.90	14.06	14.61
24-Oct	8.10	10.37	10.53	11.08	7.13	9.40	9.56	10.11
25-Oct	3.80	6.07	6.23	6.78	2.83	5.10	5.26	5.81
26-Oct	22.00	24.27	24.43	24.98	21.03	23.30	23.46	24.01
27-Oct	0.20	2.47	2.63	3.18	-0.77	1.50	1.66	2.21
28-Oct	43.10	52.80	52.80	59.26	42.13	51.83	51.83	58.29
29-Oct	0.00	0.00	0.00	0.00	-0.97	-0.97	-0.97	-0.97
30-Oct	18.30	20.57	20.73	21.28	17.33	19.60	19.76	20.31
31-Oct	10.90	13.17	13.33	13.88	9.93	12.20	12.36	12.91

Table D.4. Safety factor for the entire slope and suction for point A and B for the reference year 2006 and the future cases in scenario 2.

	Safety factor [-]		Suction [kPa]			
	2006	2011-2100	2006 point A	2011-2100 point A	2006 point B	2011-2100 point B
01-Oct	1.617	1.616	12.572	12.580	0.774	0.510
02-Oct	1.611	1.610	9.086	9.066	0.331	0.209
03-Oct	1.503	1.536	6.554	6.502	0.104	0.021
04-Oct	1.619	1.382	6.478	4.731	10.270	0.000
05-Oct	1.607	1.342	5.127	3.433	0.036	0.000
06-Oct	1.401	1.258	3.595	2.435	0.000	0.000
07-Oct	1.315	1.219	2.478	1.657	0.000	0.000
08-Oct	1.551	1.493	3.413	2.831	10.280	10.290
09-Oct	1.614	1.329	4.284	2.173	10.250	0.000
10-Oct	1.616	1.500	4.898	2.975	10.190	10.290
11-Oct	1.614	1.336	5.288	2.135	10.150	0.000
12-Oct	1.611	1.493	5.536	2.856	10.130	10.290
13-Oct	1.612	1.558	5.696	3.649	10.120	10.260
14-Oct	1.613	1.608	5.800	4.243	10.110	10.220
15-Oct	1.611	1.609	5.866	4.640	10.110	10.180
16-Oct	1.608	1.610	5.908	4.909	10.100	10.160
17-Oct	1.609	1.609	5.933	5.097	10.100	10.150
18-Oct	1.577	1.479	4.306	3.572	0.019	0.000
19-Oct	1.610	1.325	4.321	1.827	10.280	0.000
20-Oct	1.452	1.174	3.025	0.684	0.000	0.031
21-Oct	1.303	1.176	1.567	0.147	0.000	0.000
22-Oct	1.224	1.149	0.637	0.000	0.028	0.000
23-Oct	1.188	1.112	0.158	0.000	0.000	0.000
24-Oct	1.170	1.066	0.000	0.000	0.000	0.000
25-Oct	1.145	1.030	0.000	0.000	0.000	0.000
26-Oct	1.092	1.011	0.000	0.000	0.000	0.000
27-Oct	1.318	0.984	0.884	0.000	10.300	0.000
28-Oct	1.168	1.000	0.159	0.000	0.023	0.744
29-Oct	1.338	1.230	1.127	0.000	10.300	10.320
30-Oct	1.108	1.080	0.293	0.000	0.000	0.000
31-Oct	1.075	0.979	0.000	0.000	0.000	0.000